Chapter 10
Advances in Estimating the Geologic CO_2 Storage Capacity of the Madison Limestone and Weber Sandstone on the Rock Springs Uplift by Utilizing Detailed 3-D Reservoir Characterization and Geologic Uncertainty Reduction

Zunsheng Jiao and Ronald C. Surdam

Abstract In order to implement CO_2 storage in deep saline aquifers a diverse set of geologic, geophysical, and geochemical parameters must be characterized in both the targeted reservoir intervals and at the storage site.

All observational, experimental and theoretical information and laboratory measurements are integrated into a comprehensive geologic model in order to obtain an accurate characterization of a specific set of potential storage reservoirs and a targeted storage site. The integration is achieved through a series of performance assessments for a diverse set of storage scenarios utilizing numerical simulation techniques. Two of the important fluid-flow parameters that are investigated with the numerical simulations are CO_2 storage capacity and CO_2 injectivity. Reliable estimates of these two parameters are essential to both governments making energy policies and environmental regulations, and to industry trying to make quality business decisions.

Three analytical techniques are utilized to evaluate CO_2 storage capacity in both the Madison Limestone and Weber Sandstone on the Rock Springs Uplift: (1) a static volumetric approach, (2) a dynamic fluid-flow simulation approach using a homogenous reservoir model, and (3) a dynamic fluid-flow simulation approach using a more realistic 3-D heterogeneous reservoir model. The results from these three approaches demonstrate how as the descriptive characterization of the spatial distribution of the determinative reservoir parameters become more realistic, the uncertainties of the CO_2 storage performance assessments are substantially reduced.

Using comprehensive regional geologic, structural, geochemical, log suite, core, and seismic data, we present field-scale heterogeneous reservoir models for the Madison Limestone and Weber Sandstone on the Rock Springs Uplift (RSU). These

Z. Jiao (✉) · R. C. Surdam
Carbon Management Institute Laramie, University of Wyoming, Laramie, USA
e-mail: JJiao@uwyo.edu

R. C. Surdam
e-mail: rsurdam@uwyo.edu

R. C. Surdam (ed.), *Geological CO_2 Storage Characterization,*
Springer Environmental Science and Engineering, DOI 10.1007/978-1-4614-5788-6_10,

models were used to evaluate uncertainty in critical geologic carbon storage (GCS) performance metrics: storage capacity and well injectivity. The geologic setting of the RSU is presented first and is followed by a description of the techniques used to determine porosity and permeability heterogeneity based on analytic results from log suites, cores, and 3-D seismic data. Random realizations of permeability and porosity (i.e., extrapolations of reservoir properties away from the stratigraphic well into the 3-D seismic volume) are then generated for each of the geologic units including the storage targets (the Weber Sandstone and the Madison Limestone) and sealing formations (the Amsden, Dinwoody, and Chugwater, among others). These heterogeneous property fields then are used to simulate non-isothermal CO_2 injection over a 50-year period.

10.1 Introduction

Since the beginning of the industrial revolution the amount of anthropogenic CO_2 emitted into the atmosphere has risen dramatically as the utilization of fossil fuels has continually increased. Presently the atmospheric CO_2 concentration has reached 400 ppm, whereas in 1,850 it was 280 ppm—CO_2 is being pumped into the atmosphere at ever-increasing rates. Although several CO_2 mitigation schemes have been proposed, such as CO_2 storage in deep ocean settings, coal beds, depleted oil/gas reservoirs, and deep saline aquifers, the storage of anthropogenic CO_2 in deep saline aquifers is favored by a global scientific consensus. In order to implement CO_2 storage in deep saline aquifers, a diverse set of geologic, geophysical, and geochemical parameters must be characterized both in the targeted reservoir intervals and at the overall targeted storage site.

The objective of this chapter is to integrate all available observational, experimental, and theoretical information and laboratory measurements in order to accurately characterize a specific set of potential storage reservoirs and a storage site. The integration is achieved through a series of performance assessments for a diverse set of storage scenarios utilizing numerical simulations. Two important fluid-flow parameters that are investigated with the numerical simulations are CO_2 storage capacity and CO_2 injection rate. Reliable estimates of these two parameters are essential both to governments drafting energy policies and environmental regulations and to industries making business decisions.

Three simulation approaches are utilized to evaluate CO_2 storage capacity in the Madison Limestone and Weber Sandstone on the Rock Springs Uplift (RSU): (1) a static volumetric approach, (2) a dynamic fluid-flow simulation approach using a homogenous reservoir model, and (3) a dynamic fluid-flow simulation approach using a more realistic 3-D heterogeneous reservoir model. The results from these three approaches demonstrate that as the descriptive characterizations of the spatial distribution of the determinative reservoir parameters become more realistic, the uncertainty implicit in the CO_2 storage performance assessments is substantially reduced.

In this chapter, using comprehensive regional geologic, structural, geochemical, log suite, core, and seismic data, we develop a field-scale heterogeneous reservoir model for the Madison Limestone and Weber Sandstone on the Rock Springs Uplift. This model is used to evaluate uncertainty in critical geologic carbon storage (GCS) performance metrics: storage capacity and well injectivity. A brief account of the geologic setting of the RSU is followed by a description of the techniques used to determine porosity and permeability heterogeneity based on analytic results from log suites, cores, and 3-D seismic data. Realistic determinations of permeability and porosity (extrapolations of reservoir properties away from the stratigraphic well and into the 3-D seismic volume) are then generated for each geologic unit, especially the storage targets within the Weber Sandstone and Madison Limestone and the primary sealing units—the Amsden, Dinwoody/Red Peak, and Chugwater Formations. These heterogeneous property fields are then used to simulate non-isothermal CO_2 injection over 50 years.

10.2 Geologic Setting of the Rock Springs Uplift, Wyoming

The Rock Springs Uplift (RSU) has been identified as a large potential geologic CO_2 storage site in southwestern Wyoming, with initial estimates of storage capacity for the Weber Sandstone and Madison Limestone on the order of 18 billion tonnes (Gt) and 8 Gt of CO_2, respectively, using the Futuregen Protocol (Fig. 10.1a) (Surdam and Jiao 2007). The 2.3-GW Jim Bridger Power Plant located on the RSU has the largest carbon footprint in Wyoming and generates approximately 15 Mt/yr of CO_2.

The RSU is an asymmetric, doubly plunging anticline/dome with more than 3,000 m of closed structural relief (Surdam and Jiao 2007) that lies on Rocky Mountain foreland basement. This large, north–south trending, complex uplift separates the Greater Green River Basin into two parts: to the west are the Green River and Bridger Basins; to the east are the Washakie and Great Divide Basins. The size of RSU is 80 km long, south to north and 50 km wide, west to east. The western flank of the RSU dips more steeply than its eastern flank (Fig. 10.1b). There are numerous east- and northeast-trending faults cutting the RSU on the surface, and a major westward-oriented thrust fault on the western flank occurs at depth below the surface (Fig. 10.1); it is thought to be a sealed fault (Surdam and Jiao 2007).

The oldest rocks composing the RSU are the Precambrian metamorphic basement, above which are Paleozoic, Mesozoic and Cenozoic formations (Fig. 10.1c), (Surdam et al. 2009). The oldest rocks exposed on the RSU are Cretaceous marine shales and sandstones, for the Laramide tectonic event that formed the RSU during Late Cretaceous and early Tertiary times did not raise the RSU high enough to expose the Precambrian core.

The targeted saline CO_2 storage aquifers are the Weber Sandstone, 200 m thick, and Madison limestone, 130 m thick at CMI's RSU #1 well site on the eastern flank of the RSU. The Pennsylvanian Weber Sandstone is composed of fine- to medium-

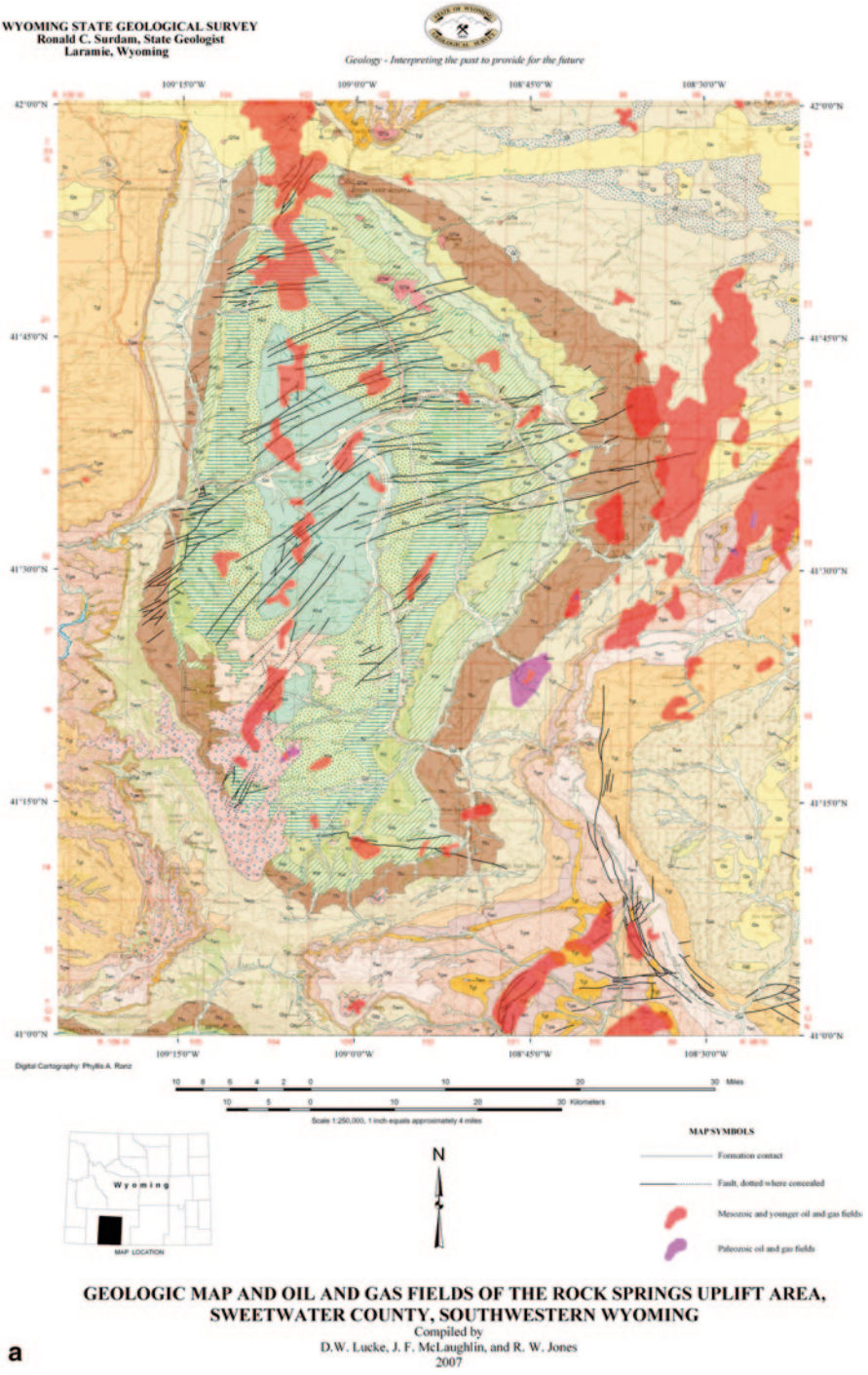

Fig. 10.1 (**a**) Geologic map of the Rock Springs Uplift, southwest Wyoming. (**b**) East-west structural cross section through the RSU. (**c**) General stratigraphic chart for the Green River Basin where the RSU is located. (Modified from Love et al. (1993))

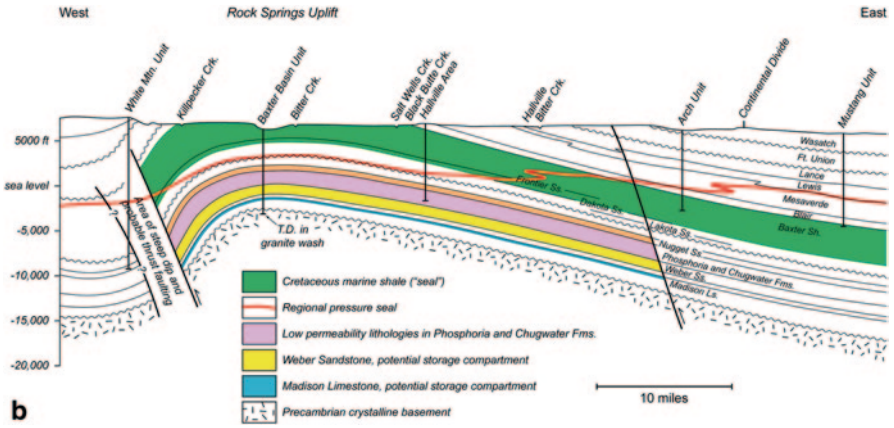

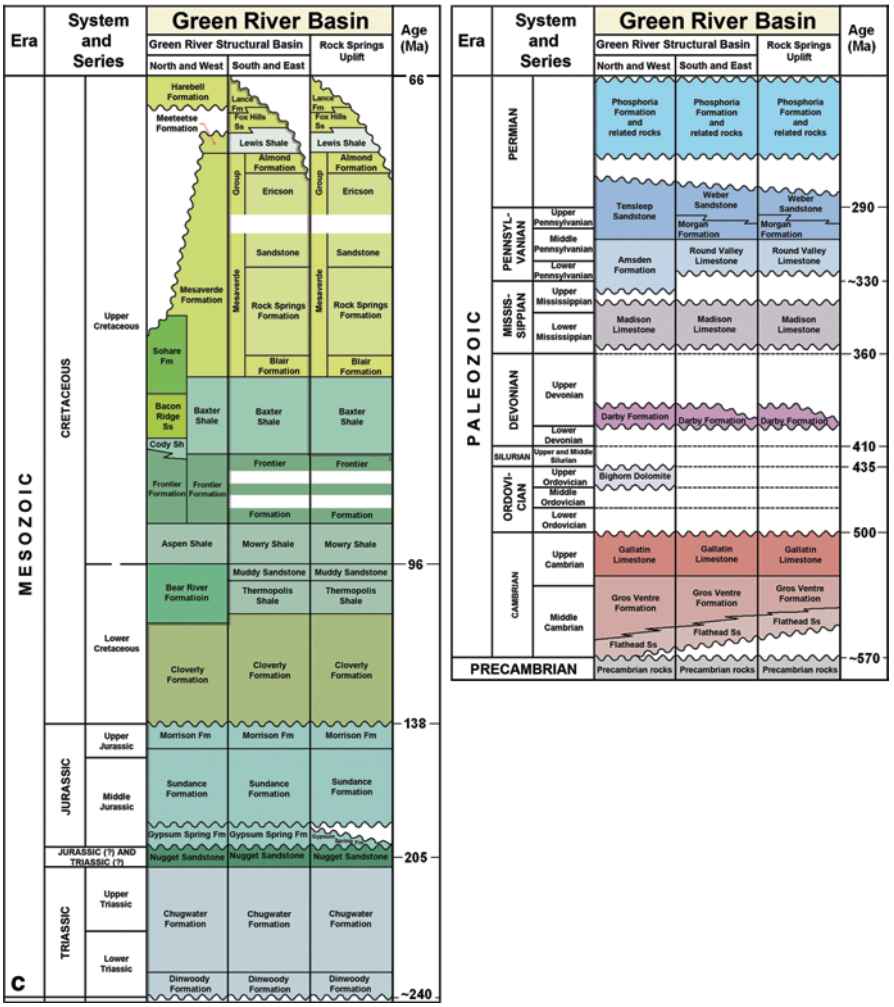

Fig. 10.1 (continued)

grained, cross-bedded sandstone and siltstone primarily deposited as sand dunes and interdunes for the upper portion, and shallow marine for the lower portion. The Mississippian Madison Limestone consists of massive limestone and dolostone deposited in a shallow marine environment. At the crest of the RSU the Weber Sandstone and Madison Limestone are 1,860 m and 2,250 m below the land surface, respectively. At the RSU #1 well site the Weber and Madison tops are 3,300 m and 3,726 m deep.

The primary caprock for the Weber Sandstone and Madison Limestone is the Triassic Dinwoody and Chugwater siltstone and shale, a thick, low-permeability stratigraphic unit (300–400 m thick) that consists of interbedded red siltstone, shale, and fine-grained sandstone (Clarey and Thompson 2010; Surdam et al. 2009). Above the primary sealing lithologies of the Dinwoody and Chugwater Formations are more than 1,500 m of Cretaceous marine shale that serve as secondary cap-rock sealing units (Surdam and Jiao 2007).

The Permian Phosphoria Formation lies between the targeted CO_2 storage reservoir within the Weber Sandstone and the Dinwoody Formation primary seal, and varies in lithology from shaly siltstone to limestone interbedded with dolomite/siltstone. The Phosphoria on the RSU represents a lithofacies transition from organic, chert- and phosphorite-rich black shale west of the RSU to carbonate east of the RSU (Hein et al. 2004; Piper and Link 2002). Therefore, the Phosphoria Formation can serve as source rock, storage reservoir, or cap rock depending on its local lithology.

The total dissolved solids (TDS) in the Weber Sandstone water ranges from 70,000 mg/l to 100,000 mg/l, and in Madison water the TDS ranges 90,000–110,000 mg/l on the RSU. There are no outcrops of the Weber Sandstone and the Madison Limestone near the RSU, and groundwater recharge areas are at least 50–100 mi (80–160 km) away from the RSU, based on nearest outcrops (Surdam et al. 2009). The relatively high TDS in these saline aquifers indicates that the targeted CO_2 storage reservoirs are compartmentalized and are not connected directly to shallow meteoric recharge. The oil and gas produced from the Cretaceous Mesaverde and Frontier Formations and the Jurassic Nugget Formations predicts the integrity of the sealing stratigraphic intervals on the RSU.

The advantages of the RSU as a site for CCS are the thickness of the storage formations, burial depth, multiple cap-rock sealing units, huge structural closure, and proximity to substantial CO_2 emission sources (Surdam and Jiao 2007).

10.3 Storage Capacity Based on the Volumetric Approach

In order to assess the pore volumes of the targeted Weber and Madison reservoirs, the Carbon Management Institute (CMI) constructed a 3-D geologic model of the RSU based on geophysical logs from oil and gas wells, 2-D seismic profiles, and regional geologic data assembled by the Wyoming State Geologic Survey and CMI. The model covers a 90-km × 122-km area that includes all or parts of Townships 12–24 north and Ranges 95–106 west; it is 7.56 km in depth (Fig. 10.1a). The model

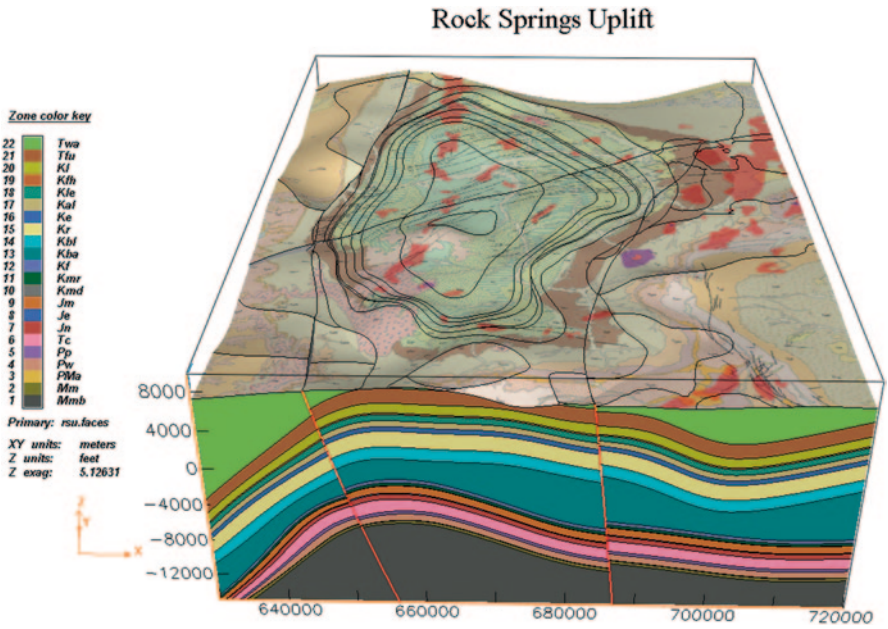

Fig. 10.2 Geologic structural model of the Rock Springs Uplift area

was built using EarthVison®, a commercial 3-D geospatial modeling software package. Most well total depths (TDs) are in Cretaceous-age formations (e.g., 736 in the Frontier Formation); just 55 wells penetrate the Weber Sandstone, and 14 wells penetrate the Madison Limestone, in the 11,000-km^2 (4,200 mi^2) model area. The formation tops below the Cretaceous are mainly extrapolated from interpreted 2-D seismic reflections and from well logs from the deep wells that penetrate the targeted formations. Based on regional geologic maps and cross sections, three major faults are included in this geologic structural model. The gridding on the X, Y, and Z axes (width, length, and depth) is $41 \times 41 \times 41$, giving $40 \times 40 \times 40$ cells (64,000 cells). The cell size is 2,250 m wide, 3,050 m long, and 189 m deep. The model was constructed using 2-D and 3-D minimum tension gridding. Figure 10.2 is a northbound oblique view of the geologic structural model of the Rock Springs Uplift area.

Burress et al. (2009) provide a formula for assessing CO_2 storage capacity based on the total known volume (TKV). The TKV is the total volume of pore space within a reservoir. The formula for the S_{TKV}, the CO_2 storage capacity in tonnes, based on the KTV is:

$$S_{TKV} = T_a \times T_i \times N_{tp} \times \Phi \times C_e \times C_f \times \rho_{co_2}, \tag{10.1}$$

where S_{TKV} is the storage resource of the assessed reservoir [t]; T_a is the trap area [m^2]; T_i is the interval thickness of the storage formation [m]; N_{tp} is the fraction of T_i occupied by the reservoir interval(s) [decimal fraction]; ϕ is the porosity [decimal

fraction]; C_e is the storage efficiency factor (the fraction of the pore space that can be occupied by CO_2) [decimal fraction]; C_f is a units conversion factor (here, $C_f = 1$); and ρ_{CO_2} is the density of CO_2 [t/m^3].

In order to use Eq. 10.1 to calculate the CO_2 storage capacity of the Weber Sandstone and Madison Limestone, the trap area (T_a)—and thickness of the targeted formations (T_i) must first be defined. In other words, we must determine the upper depth limit and the lower depth limit of the targeted reservoir. The pressure and temperature required for CO_2 to be a supercritical fluid (31 °C and 7.4 MPa) are typically met at depths greater than 800 m (2,600 ft) under a normal hydrostatic pressure gradient. To reduce the chance that CO_2 may migrate to pressure regime and temperature conditions where it could convert from the supercritical state to liquid and vapor, a minimum storage depth of 1,000 m (3,280 ft) was chosen in the study. The minimum storage depth sets the upper depth limit of a potential CO_2 reservoir. The Weber Sandstone at the crest of the RSU is buried at a depth of 5,200 ft (1,600 m), so both the Weber and Madison reservoirs meet the minimum pressure and temperature requirements for keeping the stored CO_2 in the supercritical condition. The lower depth limit for CO_2 storage is more arbitrary than the upper depth limit. If the CO_2 pressure at the wellhead is 18 MPa (2,610 psi), and CO_2 density is 0.65 g/cm^3, the CO_2 pressure will be 50.5 MPa (7,322 psi) at the bottom of a 5,000-m-deep (16,400 ft) well. Therefore, CO_2 injected at the depth 5,000 m will displace normally pressured formation water (50 MPa or 7,200 psi) without additional compression. ExxonMobil Petroleum Company has injected 1.2 Mt of mixed gas (CO_2 and H_2S) annually into two Madison Limestone wells at depth of 17,500 ft (5,330 m) since 2004 at Shute Creek, northwest of RSU. Taking these two wells as an analogous case, 5 km (16,400 ft) was chosen for the maximum storage depth.

Assuming that 100 % of the formation thickness is available for CO_2 storage ($N_{tp} = 1$), then a 412-km^3 total volume of rock and pore space available for the CO_2 storage ($T_a \times T_i \times N_{tp}$) is determined from the EarthVision® geologic structural model for the Weber Sandstone on the RSU. For the Madison Limestone, the total volume of rock and pore space is 179 km^3.

The porosities ϕ of the Weber Sandstone and Madison Limestone were determined from apparent density porosities and neutron porosities derived from available logs. For the Weber Sandstone, a lognormal porosity distribution with maximum 0.12, minimum 0.01, mean 0.05, standard deviation 0.02, and skewness 0.13 was determined from all available measured data (Fig. 10.3a). For the Madison Limestone, the lognormal porosity distribution with maximum 0.18, minimum 0.01, mean 0.09, standard deviation 0.04, and skewness 0.1 was determined from all available measured data (Fig. 10.3b).

For a saline aquifer, the upper limit on the storage efficiency factor C_e is related to the irreducible water saturation of the trap in the presence of CO_2. Values for irreducible water saturation in petroleum reservoirs are not well known, but they probably range from a minimum of about 0.2 in gas reservoirs to about 0.6 in oil reservoirs. The results of the CO_2 injection simulation, using FEHM software, presented in Sect. 10.4 show that most CO_2 saturation ranges between 0.1 and 0.8. The storage efficiency in this study was chosen between 0.1 and 0.8, with distribu-

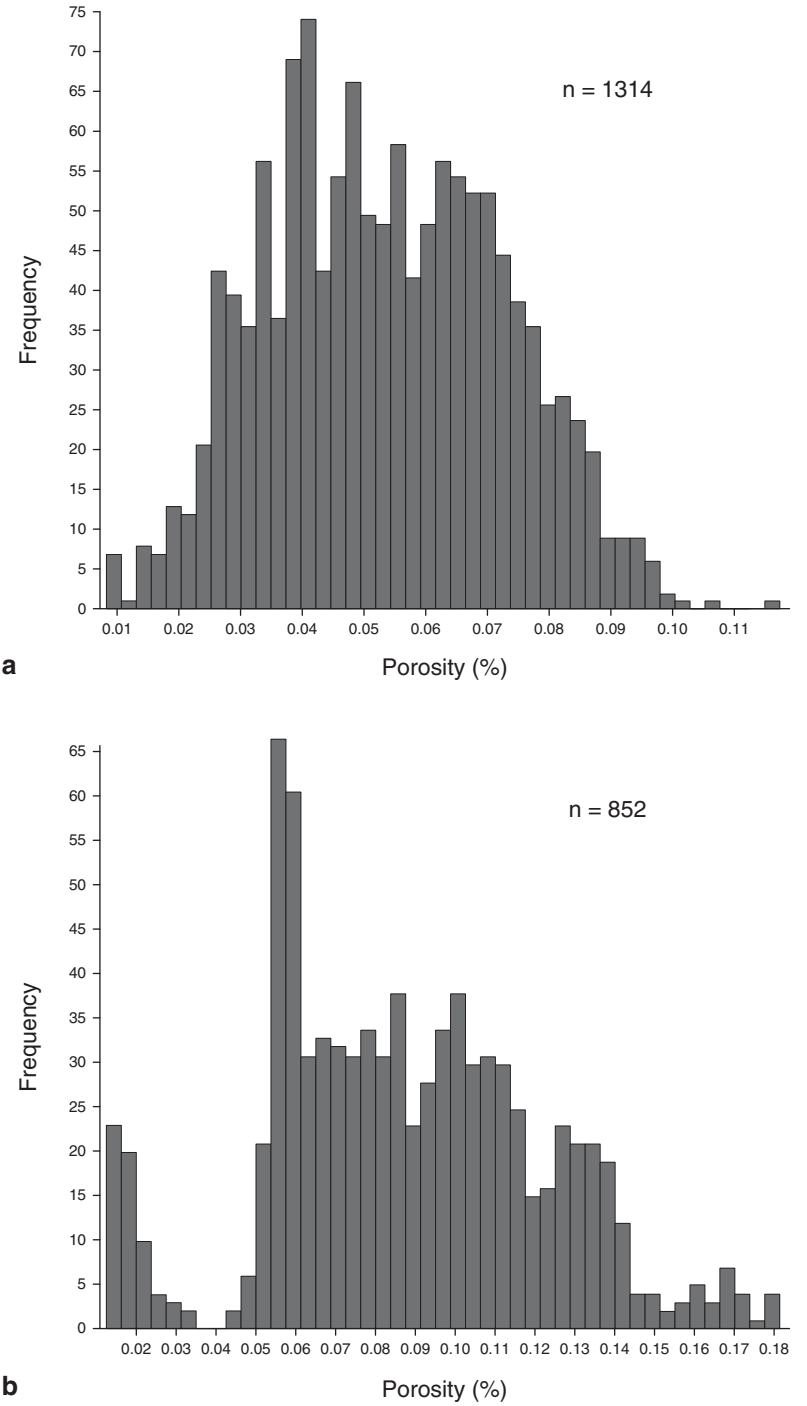

Fig. 10.3 Histograms of the density-neutron porosity of (**a**) the Weber Sandstone and (**b**) the Madison Limestone, Rock Springs Uplift

tion mean 0.66. Using these parameters, a Monte Carlo simulator from Goldsim software with 5,000 realizations was set up for the Weber Sandstone and Madison Limestone between depths of 1,000 m (elevation 1,070 m) and 5,000 m (elevation –2,930 m) on the RSU. Figure 10.4a shows the probability density of the CO_2 storage capacity of the Weber Sandstone on the RSU: the Weber CO_2 storage capacity ranges from 2.4 to 20 Gt, with a mean of 9 Gt. For the Madison Limestone, the probability density of the CO_2 storage capacity ranges from 1.6 to 14 Gt, with a mean of 6.5 Gt (Fig. 10.4b).

Therefore, on the basis of the volumetric approach the Weber Sandstone and Madison Limestone have sufficient storage capacity to accommodate decades of industrial CO_2 emissions in the Greater Green River Basin.

10.4 Storage Capacity Assessments Based on the Numerical Simulation Utilizing a Homogeneous Reservoir Model

Although the storage capacity estimates based on the volumetric approach in Sect. 10.3 are acceptable for rough screening calculations, they cannot capture the complexities of three-dimensional flow and transport involving reservoir properties, seal integrity, CO_2 dissolution, inclined geologic units, and variable pressures and temperatures leading to changes in density and viscosity of both the brine and CO_2. In this and the following sections, the focus is on a 3-D numerical model (volume simulation) congruent with the Jim Bridger 3-D 8 km × 8 km seismic survey. Focusing on this volume with a stratigraphic test well in the center of the domain allows clear illustration of how results from numerical simulations lead to better understanding of injection feasibility, storage capacity, seal integrity, and possible flow and transport issues surrounding the injection of CO_2 into the Weber Sandstone and Madison Limestone on the RSU.

10.4.1 Generation of the 3-D Computational Hydrostratigraphic Model

The focused geologic structural model is located one mile south of the Jim Bridger power plant, and consists of a block 8 km × 8 km in map view, with elevation extending from sea-level to 2420 m below sea-level (Fig. 10.5a). Following the logic and methodology outlined by Miller et al. (2007), a computational hydrostratigraphic model that maintains sharp material interfaces between the units of interest was generated from the geologic structural model. In this model, the Voronoi volume elements are aligned to follow the curvature of the unit interfaces and do not stair-step in the manner of a traditional finite element grid (see Miller et al. 2007). This allows more accurate calculation of CO_2 moving along the caprock in the up-dip

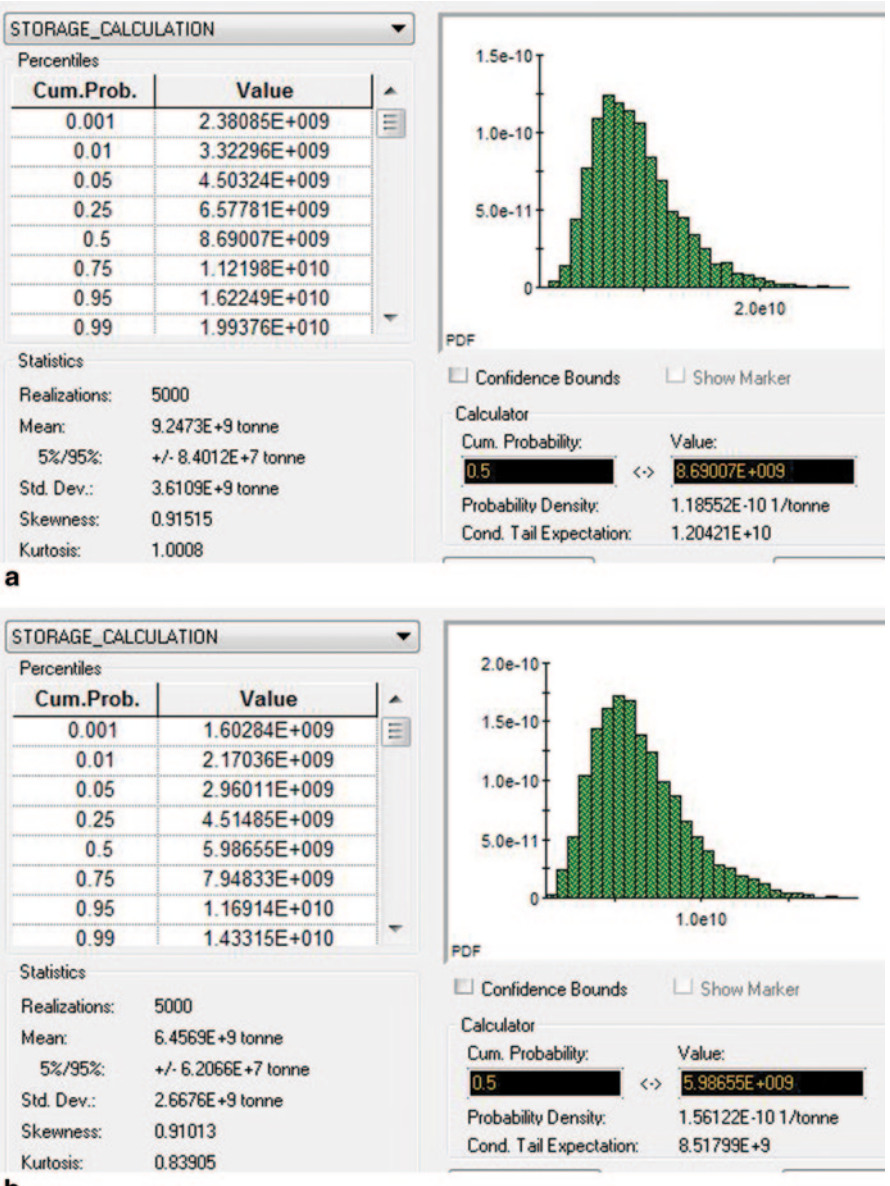

Fig. 10.4 (**a**) Probability density of the CO_2 storage capacity of the Weber Sandstone in the RSU. A cumulative probability of 25 % yields a value of 6.6 Gt. This indicates that for this particular distribution, we have a 25 % chance of storing 6.6 Gt of CO_2 or less. Put another way, this indicates that we have a 75 % chance of storing at least 6.6 Gt CO_2 in the Weber Sandstone on the RSU. (**b**) Probability density of the CO_2 storage capacity of the Madison Limestone on the RSU. A cumulative probability of 25 % yields a value of 4.5 Gt. This indicates that we have a 75 % chance of storing at least 4.5 Gt CO_2 in the Madison Limestone on the RSU

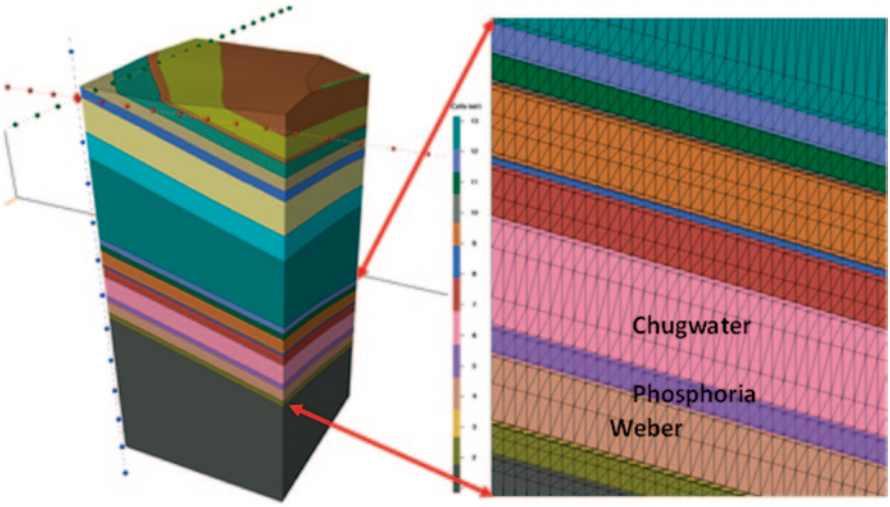

Fig. 10.5 Cross section of the hydrostratigraphic model showing the map view location of the Jim Bridger Power Plant and enlarged view of the numerical mesh in the region of interest for injection into the Weber sandstone. Horizontal grid spacing is 200 m

direction. Grid spacing is 200 m in the X and Y directions and variable in the vertical Z direction (the average vertical spacing within the targeted reservoir Weber Sandstone and Madison Limestone is 7.5 m), with 255,879 nodes and 1.6 million volume elements (Fig. 10.5b).

10.4.2 Carbon Dioxide Injection Simulation

The numerical simulations of CO_2 injection in this study were run on the Los Alamos National Laboratory multiphase porous flow simulator (finite element heat and mass transfer code, or FEHM) (Zyvoloski et al. 1988). FEHM has been used successfully for many multiphase applications including isotopic fractionation in the vadose zone, methane hydrate dissolution and transport, geothermal energy analysis, and simulations of CO_2 injection into saline aquifers (Stauffer et al. 2009a, b). The CO_2 equations of state are built into a lookup table that can capture the transition from supercritical fluid to liquid/gas across the region of discontinuous derivatives. The solubility of CO_2 in brine is determined using the model of Duan et al. (2006) and Stauffer et al. (2009a, b).

Although the Los Alamos FEHM research simulation software is used in this study other available numerical simulation software produces similar results. For example, Zhang and Qin (internal report, University of Wyoming Petroleum Engineering Department) compared the results from the FEHM simulator with those from Schlumberger's Eclipse® software for a potential CO_2 storage project involv-

ing the Madison Limestone on the Moxa Arch in Western Wyoming. The results from this study are quite similar, with no significant disparities.

Initial conditions for the targeted domain included a geothermal gradient of 26 °C/km with a bottom temperature of 123 °C and a top temperature of 60 °C, and a hydrostatic pressure gradient ranging from 21.6 MPa (3,130 psi) at the top of the domain (sea-level, depth 2,160 m) to 45.8 MPa (6,640 psi) at the bottom (depth 4,580 m). Further simplifying assumptions for the 3-D injection calculations were that the thermal conductivity of the rocks is constant at 0.5 W/mK, rock density is constant at 2,650 kg/m^3, porosities in the Weber Sandstone and Madison Limestone are both assigned at 10 %, and heat capacity is constant at 1,000 J/kgK. A CO_2 permeability of 1 mD was assigned to targeted reservoirs, the Weber Sandstone and Madison Limestone. Permeability values used in the simulations for confining formations were assigned at 0.01 mD. A residual saturation of 10 % was assigned to both brine and CO_2, using a linear relationship. Capillary pressure effects were ignored. Brine TDS is constant at 90,000 ppm for all formations, and water viscosity is calculated independently of brine content or dissolved CO_2. The initial dissolved CO_2 concentration was set at zero, as a bounding condition (The formation test report data from the region suggests that the in-situ concentration of dissolved CO_2 in the Weber and Madison brines may be greater than zero.) During CO_2 injection, the simulator allows for the possibility of CO_2 dissolution in water. For all simulations, the down-dip sides (north and east sides) of the domain were closed, whereas the up-dip sides (south and west sides) were open for the reservoir fluids to flow freely out of the simulation area. The open up-dip boundaries are an essential condition for creating accommodation space and preventing the reservoir pressure from elevating to the fracture pressure of the sealing formations. The model includes production of formation brines at the land surface at a distance up-dip from the injection well to manage pressure and to reduce fluid migration out of the study area.

10.4.3 CO_2 Injection into the Weber Sandstone

A model injection well was located in section 16, Township 20 North, Range 101 West (sec. 16, T20N, R101W). The thickness of the Weber Sandstone at this location was set at 700 ft (213 m) (657 ft measured in the RSU #1 well). Of the 27 nodes within the Weber Sandstone in the model well, 16 nodes were used for CO_2 injection. The reservoir petrophysical properties were held constant. The porosity of the Weber Sandstone was set homogeneous at 10 %, and the permeability was set homogeneous at 1 mD. The confining layers of the Amsden below and the Dinwoody, Chugwater above the Weber were assigned a permeability of 0.01 mD.

Serial injection simulations into the Weber Sandstone were performed, at injection rates of 0.5 Mt/yr, 1.0 Mt/yr, and 1.5 Mt/yr. In the simulation at 1.0 Mt/yr, 10 % porosity, and 1 mD permeability the reservoir pressure elevated quickly when injection began, remained below the hydro-fracture pressure throughout the 50 years of injection and, when injection ceased it returned to near the original reservoir

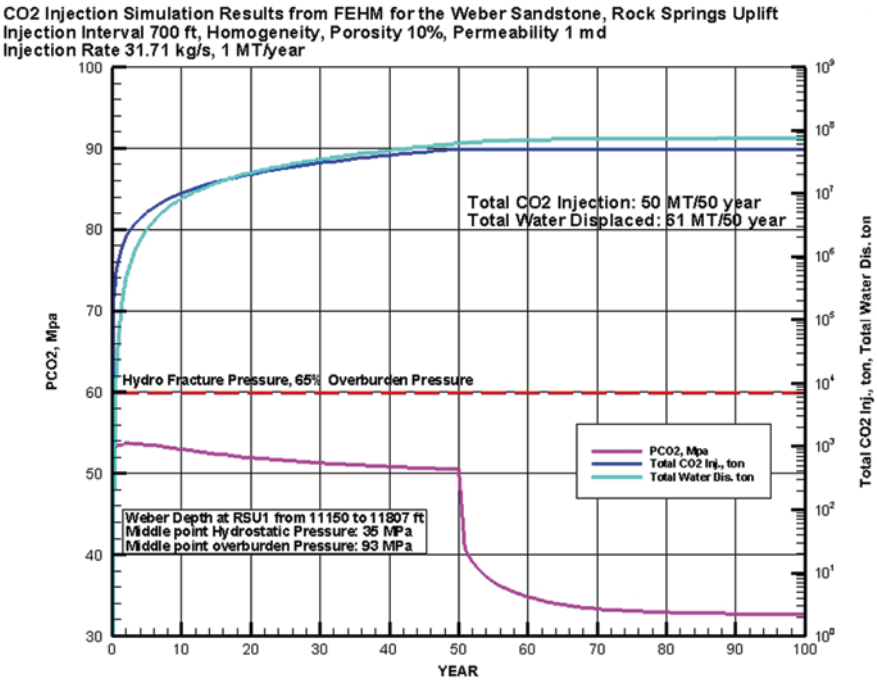

Fig. 10.6 FEHM CO_2 injection simulation results for the Weber Sandston, RSU. The simulation was set up for homogenous reservoir petrophysical conditions with 10% porosity and 1 mD relative permeability. The injection rate of 31.71 kg/s was constant for 50 years; then injection ceased, and the simulation ran for another 50 years without CO_2 injection. The reservoir pressure elevated quickly when injection began but was below the hydro-fracture pressure throughout injection. After injection ceased, the reservoir pressure fell back to near the original reservoir pressure within 10 years

pressure within 10 years (Fig. 10.6). When injection ceased at the beginning of the 51st year, 66 Mt of pore fluids had been displaced over the 50-year injection period to maintain the reservoir pressure below the hydro-fracture pressure. At an injection rate of 1.5 Mt/yr the reservoir pressure increased to the fracture pressure, and the simulation was terminated.

The plume of 1 Mt of CO_2 after 50 years of a single well injection is nearly circular, with a radius of 1,600 m, covering an area of 8 km^2 (Fig. 10.7a). Figure 10.7b is an oblique view of the injected CO_2 plume for the targeted Weber Sandstone after 50 years of injection at 1 Mt/year. The CO_2 plume has moved across the formation boundary of the Weber Sandstone into the Phosphoria Formation above and the Amsden Formation and just into the Madison Limestone below (Fig. 10.7c). The CO_2 plume with saturations from 0.05 to 0.9% and occupied a volume of 1.2 km^3. The total volume of the Weber Sandstone above a depth of 5,000 m within the RSU is 412 km^3. Therefore, if all the Weber Sandstone on the RSU were used for the storage, its storage capacity could be 17 Gt of CO_2.

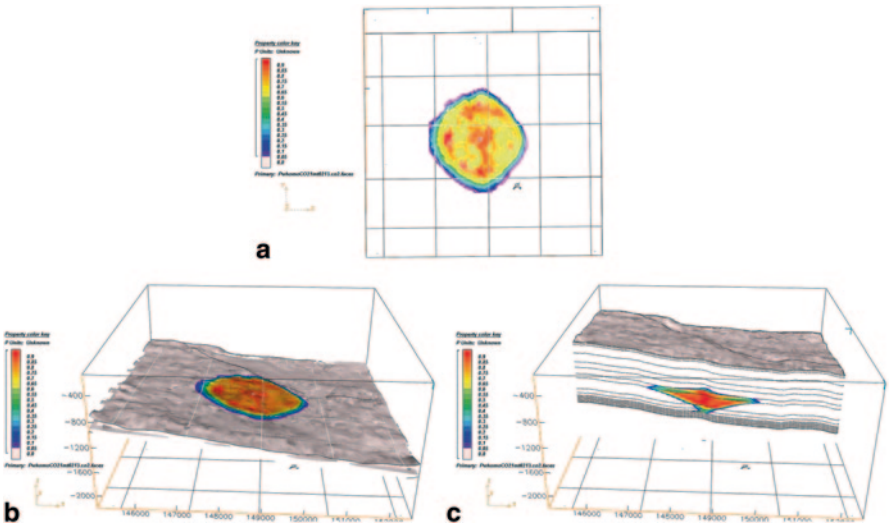

Fig. 10.7 CO_2 plume distribution in the Weber Sandstone after 50 years of injection within the Jim Bridger 3-D seismic survey area, Rock Springs Uplift. The simulation used an injection interval of 700 ft, homogenous porosity (10%) and relative permeability (1 mD), and an injection rate of 1 Mt/yr in a single injection well. The up-dip boundary is open to allow fluid displacement. After 50 years of CO_2 injection at a constant injection rate of 31.7 kg/s, the simulation continued for 50 years to let reservoir pressure dissipate and to monitor CO_2 migration. **(a)** Map view of the CO_2 plume distribution on the top of the Weber Sandstone: the plume is circular with a radius of 1,600 m. The white five-pointed star is the location of the injection well. **(b)** Oblique view. **(c)** East-west cross section

10.4.4 CO_2 Injection into the Madison Limestone

The same model injection well located in sec. 16, T20N, R101W was used for the CO_2 injection simulation into the Madison Limestone. Of the 16 nodes within the Madison Limestone interval in this well, 12 nodes were used for CO_2 injection. The thickness of the Madison Limestone at this location was set at 400 ft (122 m) (426 ft measured in the RSU #1 well). The reservoir petrophysical properties were held constant. The porosity of the Madison Limestone was set homogeneous at 10%, and the permeability was set homogeneous at 1 mD. The confining layers of the Amsden and Dinwoody-Chugwater above and the Darby below the Madison were assigned a permeability of 0.01 mD.

As with the Weber Sandstone simulations, serial injection simulations into the Madison Limestone were performed at injection rates of 0.5 Mt/yr, 1.0 Mt/yr, and 1.5 Mt/yr. For the simulation at 1.0 Mt/yr, 10% porosity, and 1 mD of permeability the reservoir pressure remained below hydro-fracture pressure (65% of the overburden pressure). The reservoir pressure increased quickly when injection started, then leveled off until injection ceased. At the ending of the 50th year 59 Mt of pore fluids had been displaced over the 50-year injection period to maintain the reservoir

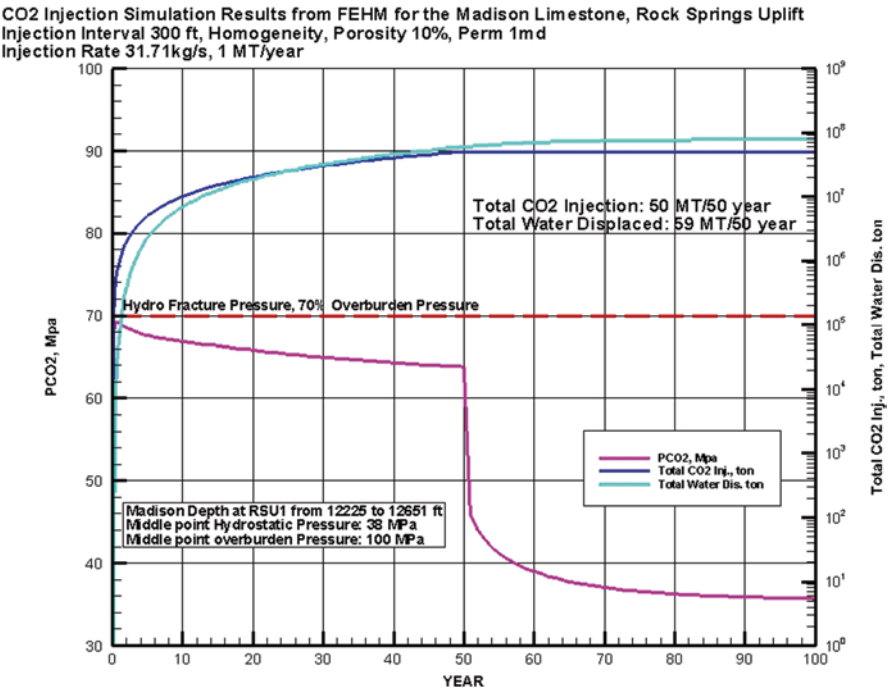

Fig. 10.8 FEHM CO_2 injection simulation results for the Madison Limestone, RSU. The simulation was set up for homogenous reservoir petrophysical conditions with 10% porosity and 1 mD relative permeability. The injection rate of 31.71 kg/s was constant for 50 years; then injection ceased, and the simulation ran for another 50 years without CO_2 injection. The reservoir pressure elevated quickly when injection began but was below the hydro-fracture pressure throughout injection. After injection ceased, the reservoir pressure fell back to near the original reservoir pressure within 10 years

pressure below the hydro-fracture pressure. After injection ceased, the reservoir pressure fell back to near the original pressure within 10 years (Fig. 10.8). The injection rate of 1.5 Mt/yr resulted in the reservoir pressure increasing to the fracture pressure, and the simulation was terminated.

The plume of 1.0 Mt CO_2 after 50 years at a single injection well is nearly circular with a radius of 1,950 m, covering an area of 12 km^2 (Fig. 10.9a). Figure 10.9b, c shows oblique and sectional views of the injected CO_2 plume for the targeted Madison Limestone after 50 years of injection at 1 Mt/yr. After 50 years of injection, the CO_2 plume has moved upward across the formation boundary of the Madison Limestone into the lower Amsden Formation. The CO_2 plume after 50 years of a single well injection with saturations from 0.05 to 0.9% occupied a volume of 1.23 km^3 within the Madison Limestone. The total volume of the Madison above a depth of 5,000 m within the RSU is 179 km^3. Therefore, if all the Madison Limestone on the RSU were used for storage, its storage capacity could be 7 Gt of CO_2.

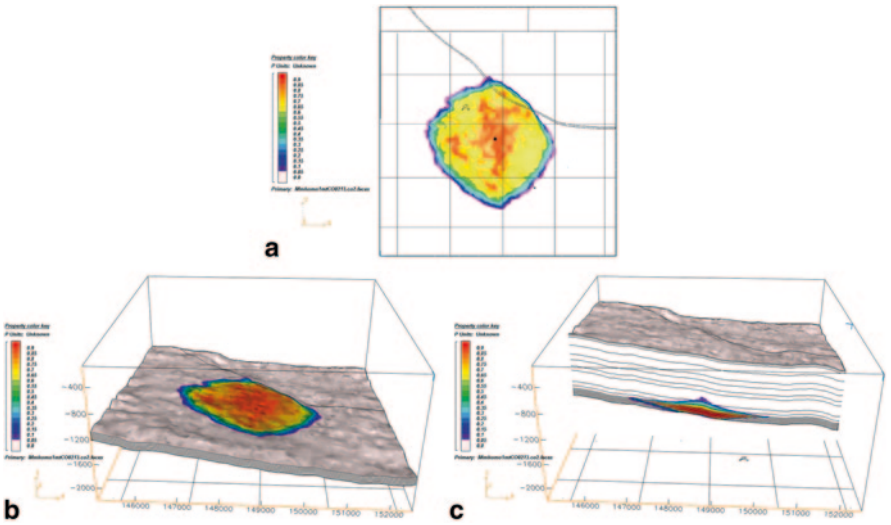

Fig. 10.9 CO_2 plume distribution in the Madison Limestone after 50 years of injection within the Jim Bridger 3-D seismic survey area, Rock Springs Uplift. The simulation used an injection interval of 400 ft, homogenous porosity (10 %) and relative permeability (1 mD), and an injection rate of 1 Mt/yr in a single injection well. The up-dip boundary is open to allow displaced fluid migration. (**a**) Map view of the CO_2 plume distribution on the top of the Madison: the plume is circular with a radius of 1,950 m. The black five-pointed star is the location of the injection well. (**b**) Oblique view. (**c**) east-west cross section

10.5 Storage Capacity Assessments Based on the Numerical Simulations Utilizing a Heterogeneous Reservoir Model

The regional geologic CO_2 storage capacity assessments and numerical CO_2 injection simulations discussed in Sects. 10.3 and 10.4 reveal that the greatest uncertainty in the quantitative assessments of the storage capacity of a selected storage site lies in characterizing geologic heterogeneity in three dimensions. Heterogeneities in the porosity and permeability of geologic CO_2 storage reservoirs and surrounding strata are the two most important factors influencing storage capacity estimates, injection feasibility, CO_2 plume migration pathway determination, sealing strata integrity, reservoir pressure and displacement fluid management, and risk assessment. To reduce the uncertainties relative to the reservoir and confirming strata properties at the RSU geologic CO_2 storage site, a stratigraphic test well was drilled, a 3-D seismic survey was acquired, and a log suite and 279 m (916 ft) of core (from the Weber Sandstone and Madison Limestone reservoir units and the Dinwoody Formation and Amsden Formation sealing units) were collected from the newly drilled stratigraphic test well. Three-dimensional data suites derived from core sedimentary facies descriptions, petrographyic observations, laboratory measurements, log analyses, and seismic attribute interpretations reduce uncertainty significantly and improve the accuracy of the numerical simulations.

10.5.1 Multi-scale Heterogeneity Characterization

This chapter takes an integrated approach to characterizing the heterogeneities of the porosity and permeability in targeted storage reservoirs and containment formations. The high-vertical-resolution core measurement data and log data were used to generate a reservoir heterogeneity property model based on the seismic attribute analysis results from the newly acquired Jim Bridger 3-D seismic survey (see Chap. 9). First the lithofacies were determined for each formation on the basis of the detailed core descriptions and petrographic observations (see Chap. 6). Second, selected core samples from each lithofacies were measured for porosity and permeability under in-situ conditions. Third, the log porosities were calibrated against the laboratory measured core porosities. Fourth, the relationship between the porosity and acoustic velocity was derived from all available logs for each of the formations. Fifth, the 3-D porosity distribution of the RSU CO_2 storage site was populated using the velocity volume of the Jim Bridger 3-D seismic survey (modeling domain) and the function relating the porosity and acoustic velocity derived from the well logs. Sixth, once spatial distributions of porosity in the modeling domain had been acquired, permeability spatial distributions based on empirical correlations between porosity and permeability were obtained. Seventh, 3-D numerical simulations of injection of CO_2 into the Weber Sandstone and Madison Limestone using the heterogeneous reservoir properties were conducted with a finite element multiphase flow simulator, FEHM (Zyvoloski et al. 1997).

10.5.2 Core Measured Porosity

Routine core analyses were conducted on 128 core plug samples from reservoir strata within Weber Sandstone and Madison Limestone, and containment strata Dinwoody Formation and Amsden Formation from the RSU #1Well. All tests were conducted by Intertek Westport Technology Center. Pore volume and permeability measurements were made with the samples mounted in a rubber-sleeved, hydrostatically loaded overburden cell. The samples were tested at 800 psi (55 MPa) and at a calculated reservoir net confining stress (NCS). Boyle's Law, using helium as the gas medium, was employed to determine pore volume. Unsteady-state Klinkenberg permeability was measured after each pore volume measurement. Permeability to air was calculated using the unsteady-state flow data.

The porosity shows significant variation within the targeted reservoirs of the Weber Sandstone and Madison Limestone (Fig. 10.10a). In the Weber Sandstone samples, porosities range from 0.7 to 8.2% under the reservoir NCS, and densities range from 2.63 to 2.7 g/cm^3. The variation of the porosity distribution in the Weber Sandstone is clearly affected by its depositional and diagenetic environments. The Middle-Late Pennsylvanian Weber Sandstone is composed of both clastic and carbonate deposits (Love et al. 1993) that can be divided into an upper eolian facies and lower shallow, warm epicontinental marine facies. The micritic limestone and

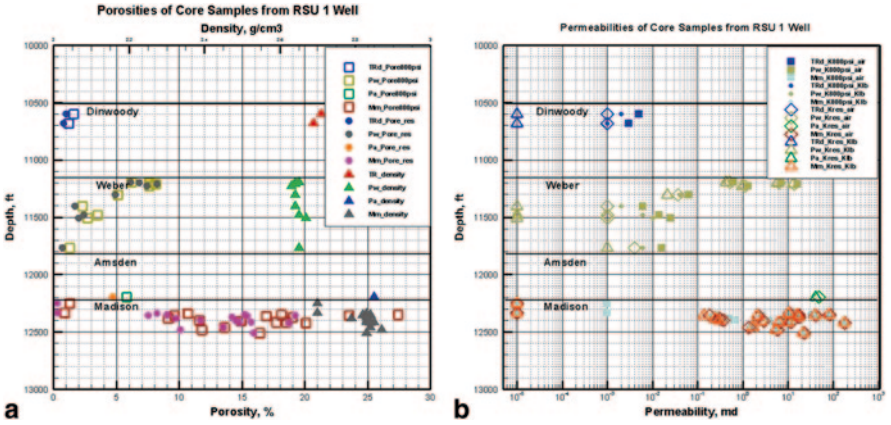

Fig. 10.10 (**a**) Plot of porosity and density versus depth for the Weber Sandstone and Madison Limestone targeted reservoirs and Dinwoody Formation and Amsden Formation containment units. Both the porosities measured under 800 psi NCS and reservoir NCS are shown. (**b**) Air and Klinkenberg permeability variations in targeted reservoirs and containment formations under 800 psi NCS and reservoir NCS

quartz sandstone in the lower marine facies are very tight; their porosity is less than 5%. The massive quartz sandstone in the upper eolian facies has relatively higher porosity, up to 10%. In the Mississippian Madison Limestone samples, porosities range from 0.3 to 19% under the reservoir NCS, and densities range from 2.7 to 2.87 g/cm^3. The porosity and permeability of the Madison Limestone is mainly controlled by the following factors: (1) dissolution associated with karst development on a regional unconformity, (2) large-scale fracturing, (3) dissolution of foram shells in the limestone and dolostone, and (4) dolomitization (see Chap. 6). The greatest variance in the porosity and permeability of the Madison limestone results primarily from the heterogeneous distribution of karstification and dolomitization.

The porosities measured in the containment strata within the Dinwoody formation are less than 1%, and their average density is 2.7 g/cm^3 (Fig. 10.10a). The porosity differences between the 800 psi NCS and reservoir NCS are less than 1% in the Weber Sandstone and Dinwoody Formation, but are significant in the Madison Limestone. The porosity difference of the Madison Limestone samples is greater than 5% (e.g., from 14 to 19% under the reservoir NCS). The significant porosity difference of the Madison Limestone under the 800 psi (5.5 MPa) NCS and reservoir NCS (>5,000 psi, 34.5 MPa) may result from two factors, higher porosity and carbonate mineralogy. The porosities measured from several samples from the Madisone Limestone are greater than 20%. These larger porosities are mostly secondary porosity.

Figure 10.10b shows the air and Klinkenberg permeability variations in both targeted reservoirs and containment formations under 800 psi (5.5 MPa) NCS and reservoir NCS. The Klinkenberg permeability in the Weber Sandstone under reservoir NCS (5,000 psi, 34.5 MPa) ranges from 0 to 12.9 mD. The higher permeability

(>1 mD) mainly shows in the upper eolian facies of the Weber Sandstone. In the Madison Limestone, the Klinkenberg permeability under reservoir NCS (5,500 psi) ranges from 0 to 16.8 mD. Several higher permeabilities (up to 183 mD) measured in the Madison Limestone are within the karst or vuggy section. The effect of net confining stress shows mainly on the lower-permeability samples. The Klinkenberg permeability under reservoir NCS can be two orders of magnitude lower than that under the 800 psi NCS in low-permeability samples.

10.5.3 Log Porosity and Core Porosity

To establish confidence in log evaluations, the porosity calculated from logs should agree with those from the core derived measurements. The porosity of a rock is a measure of its capacity to contain or store fluids, and is expressed as the pore volume of the rock divided by its bulk volume. Porosity is classified as total porosity and effective porosity. *Total porosity* is defined as all the pore space containing fluids (water, oil or gas), whether or not they are mobile. This pore space includes any hydrocarbon fluids, mobile water, capillary bound water and clay-bound water**.** *Effective porosity* is the total porosity less the fraction of the pore space occupied by cements such as silica, carbonate, or irreducible water. Because it is not possible to measure effective porosities in a reliable and repeatable manner, calibration with core analyses is best achieved by estimating total porosities from logs and comparing these with measured total porosities in core plugs.

The best way to calculate total porosity is to use the density log, correcting for lithology (using grain density) and fluid density (using invaded-zone resistivity or neutron logs). Formation bulk density is a function of matrix density, porosity, and the density of the fluid in the pores. To determine the density porosity from the bulk density log, the matrix density and density of the fluid in the pores must be known. Based on the results of laboratory core measurements from RSU #1 well, densities of 2.7 g/cm^3 for the Dinwoody Formation, 2.64 g/cm^3 for the Weber Sandstone, 2.70 g/cm^3 for limestone in the Madison Limestone, and 2.84 g/cm^3 for dolostone in the Madison Limestone g/cm^3 were chosen for the porosity estimates from the bulk density log in this study. Cross plots of the laboratory-measured porosities under reservoir conditions vs. log derived porosity show that neutron porosity overestimates the porosity of the carbonate rocks and carbonaceous shale, whereas density porosity underestimates the porosity of the carbonate rocks (Fig. 10.11a, b). As indicated by Asquith and Gibson (1982), true porosity can be calculated from neutron porosity and density porosity using a root mean square formula (gas-bearing formations) or mathematical mean formula (oil-and-water bearing formations). The heavy magenta line on Fig. 10.12 represents the total porosity estimated from the neutron and density porosity logs from the RSU #1 well. These neutron-density porosities correlate roughly with the core measured porosity (Fig. 10.11c). The neutron-density porosity still overestimates the carbonaceous shale and a few limestone samples. These effects may be caused by the high clay content in the shale and vugs

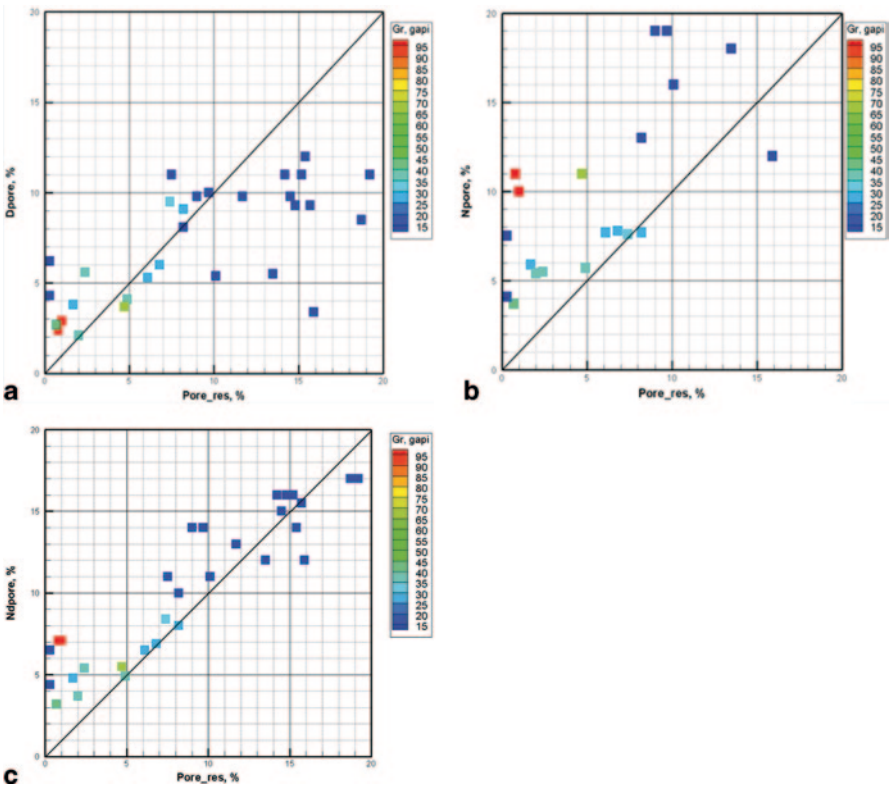

Fig. 10.11 Crossplot of the laboratory measured porosity at reservoir conditions vs. the log-derived (**a**) bulk density porosity and (**b**) neutron porosity. (**c**) Crossplot of the laboratory measured porosity at reservoir conditions vs. the log derived neutron-density porosity

in the limestone, where the porosity could be shown on the well logs but could not be measured in the laboratory.

10.5.4 Sonic Velocity and Neutron-Density Porosity

Because of the vertical extent of the borehole data used here, the vertical heterogeneity distributions are captured more fully than the horizontal ones. In order to characterize the spatial distributions of the heterogeneity properties of the targeted reservoirs and containment strata, seismic attributes must be correlated with the core and log derived petrophysical properties. Using the log suite from RSU #1 well, the relationships of the neutron-density porosity and sonic velocity were established for the Cretaceous Mowry Shale and Muddy Sandstone; the Jurassic Morrison Formation, Entrada Sandstone Member (Sundance Formation), Gypsum Spring Formation, and Nugget Sandstone; the Triassic Chugwater Formation, Red Peak Member

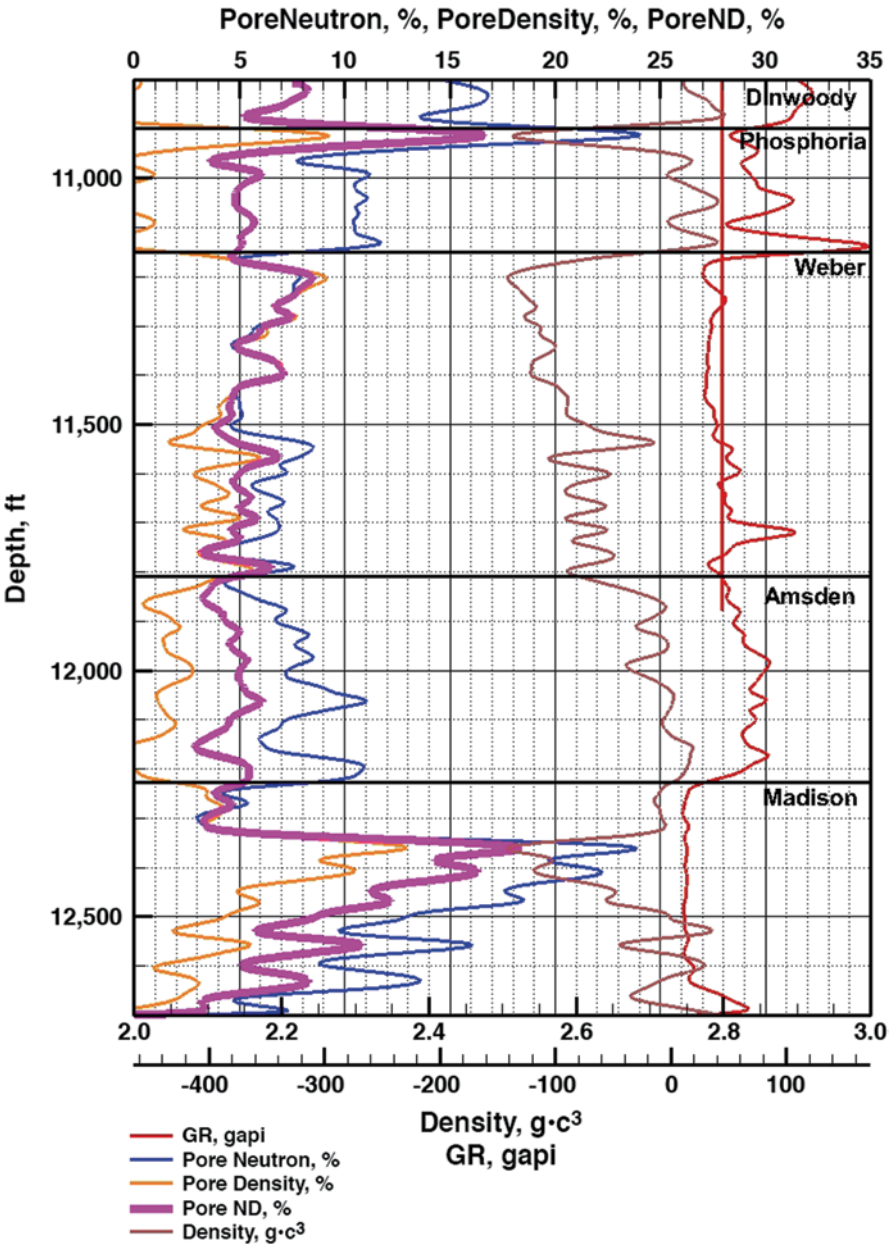

Fig. 10.12 Plots of the gamma ray, bulk density, neutron porosity, and density porosity for the Dinwoody Formation, Phosphoria Formation, Weber Sandstone, Amsden Formation and Madison Limestone from RSU #1 well logs. The heavy magenta plot is neutron-density porosity calculated from neutron and density porosity and is used to establish the function between the porosity and the sonic velocity

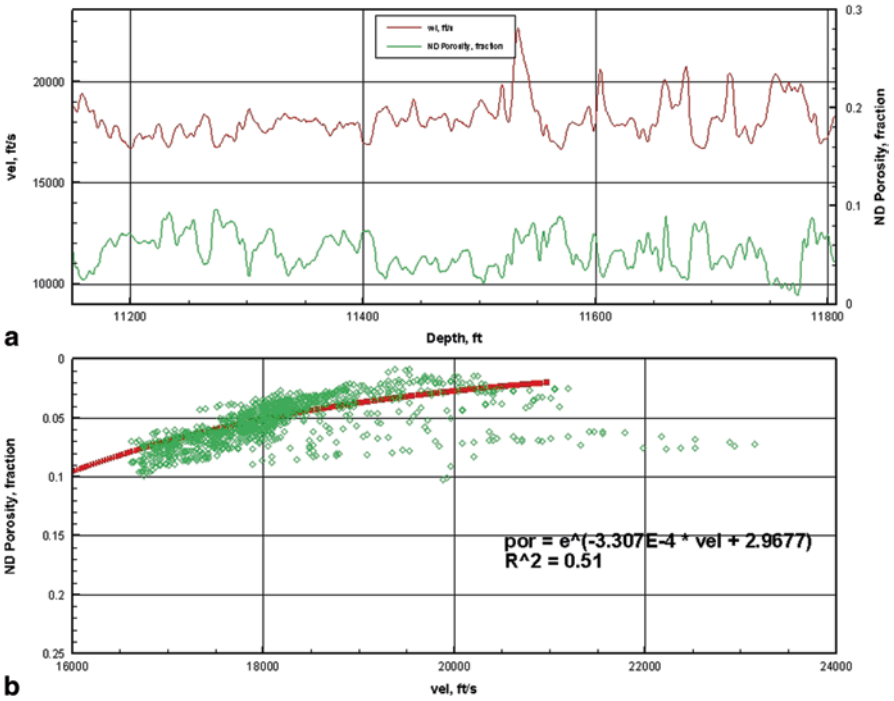

Fig. 10.13 (**a**) Smoothed sonic velocity and neutron-density porosity logs through the Weber Sandstone in the RSU #1 well. (**b**) Crossplot of the relationship between sonic velocity and neutron-density porosity in the Weber Sandstone

(Chugwater Formation), and Dinwoody Formation; the Permian Phosphoria Formation, the Pennsylvanian Weber Sandstone and Amsden Formation; the Mississppian Madison Limestone; and the Devonian Darby Formation.

The depositional environment of the Weber Sandstone was a near-shore eolian environment, and facies changes (sand dune and inter-dune) within the Weber Sandstone caused significant variations in rock porosity. Figure 10.13a shows the sonic velocity and neutron-density porosity variations of the Weber Sandstone in the RSU #1 well. The relationship between the sonic velocity and neutron-density porosity for the Weber Sandstone is shown on Fig. 10.13b. The higher porosities that plot off (below) the correlation function line are secondary, probably the result of micro fractures. The neutron-density porosities of Weber Sandstone in RSU #1 well range from 2 to 13%, with a mean of 5% (Fig. 10.14a). Applying the function shown on Fig. 10.13b, porosities derived from the sonic velocities range from 1 to 8% with a mean of 5% (Fig. 10.14b). The normal distribution of the sonic velocity (Fig. 10.14c) is comparable with the sonic-derived porosity distribution (Fig. 10.14b).

Figure 10.15a shows the sonic velocity and neutron-density porosity variations of the Madison Limestone in the RSU #1 well. The relationship between the son-

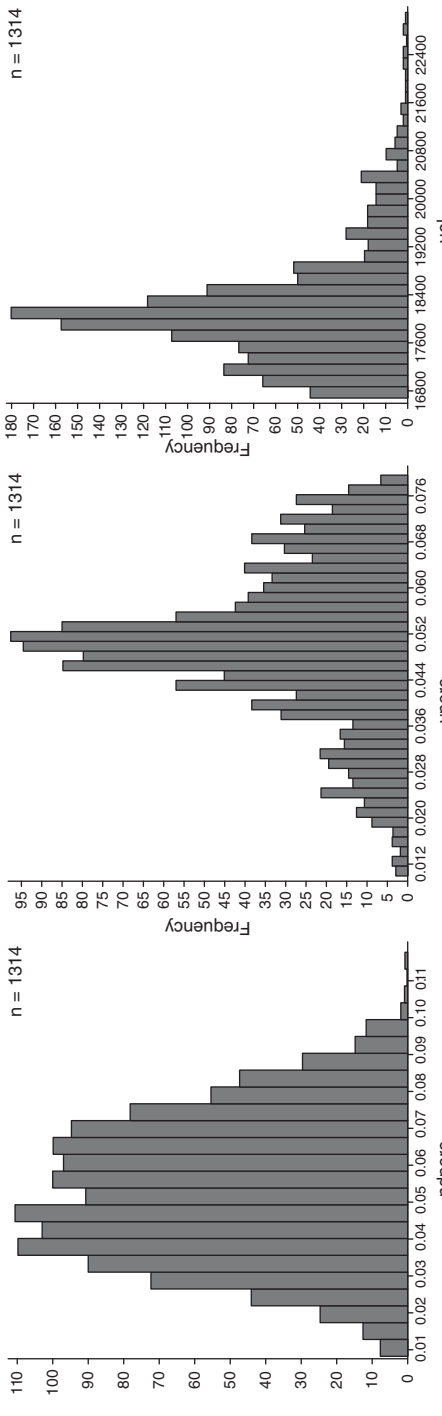

Fig. 10.14 Histograms of the neutron-density porosity of the Weber Sandstone from the RSU #1 well logs, the porosity derived from sonic velocity, and the sonic velocity from the RSU #1 well

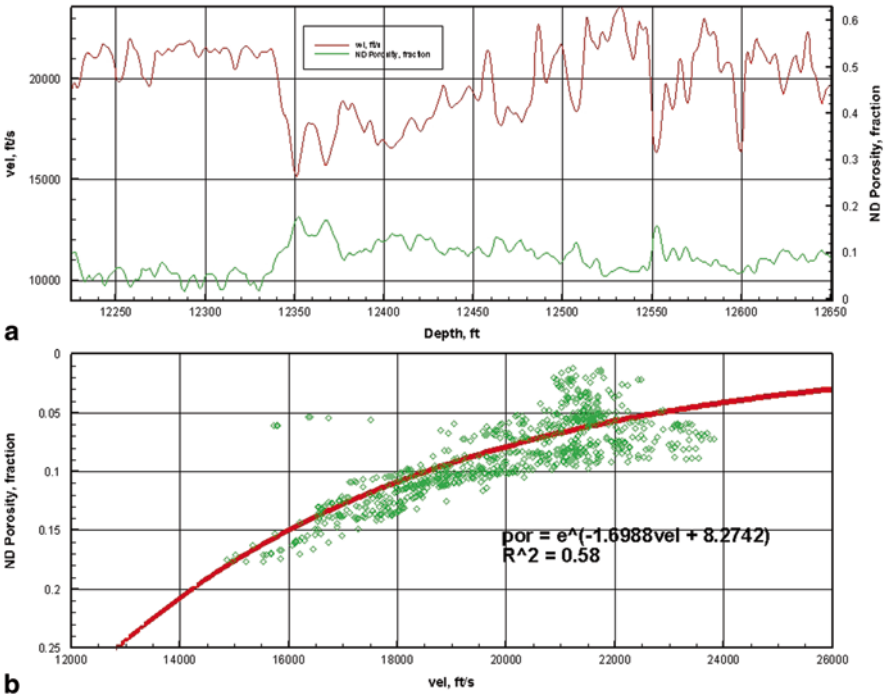

Fig. 10.15 (**a**) Smoothed sonic velocity and neutron-density porosity logs through the Madison Limestone in the RSU #1 well. (**b**) Crossplot of the relation of sonic velocity and neutron-density porosity in the Madison Limestone

ic velocity and neutron-density porosity for the Madison Limestone is shown on Fig. 10.15b. The neutron-density porosities from well logs of Madison Limestone in RSU1 well range from 1 to 18 %, with a mean of 7 % (Fig. 10.16a). Applying the function shown on Fig. 10.15b, porosities derived from the sonic velocities range from 4 to 18 %, with a mean of 8 % (Fig. 10.16b).

The research group at CMI has developed an innovative technology to construct a more accurate seismic interval velocity model from pre-stack, CMP sorted seismic gather data. This statistical approach is used to generate a more reliable 3-D interval velocity model for the Jim Bridger seismic survey (see Chap. 7). Using the sonic velocity and neutron-density porosity functions established for each formation of interest, the 3-D porosity volume for the CO_2 injection simulation domain was generated from the Jim Bridger 3-D interval velocity volume. The distributions of porosities derived from seismic interval velocities for the Weber Sandstone and Madison Limestone targeted reservoirs are shown on Figs. 10.17 and 10.18. The porosities derived from seismic interval velocities for the Weber Sandstone range from 2 to 13 % with a mean of 5 % within the Jim Bridger simulation domain (Fig. 10.17a). The porosities derived from seismic interval velocities for the Madison Limestone range from 7 to 18 % with a mean of 11 % within the Jim Bridger

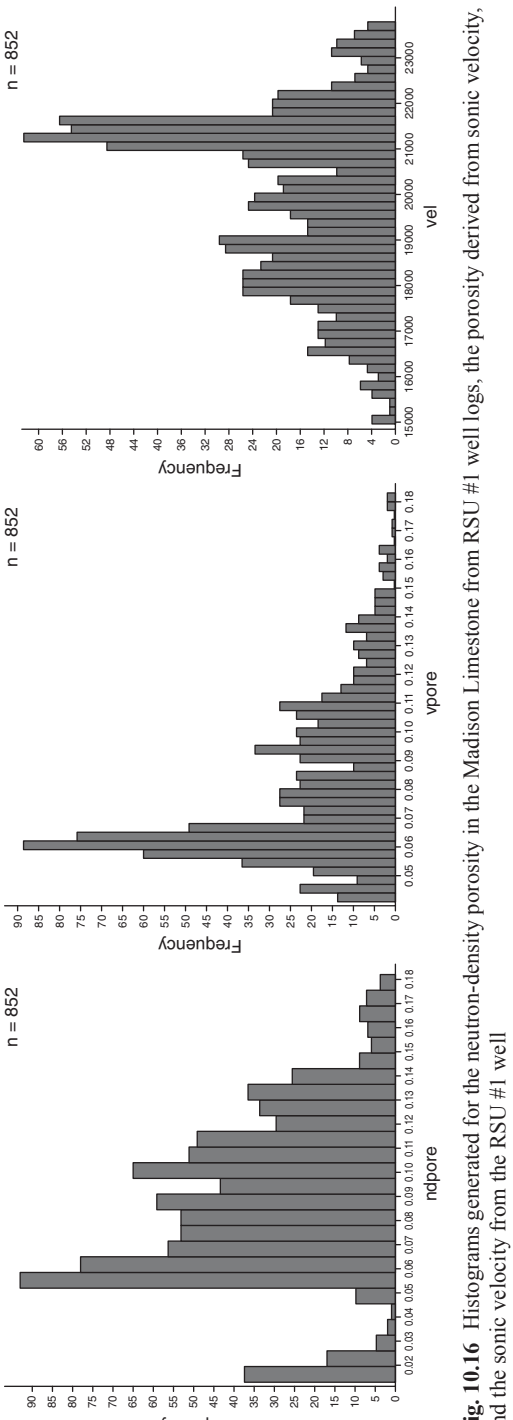

Fig. 10.16 Histograms generated for the neutron-density porosity in the Madison Limestone from RSU #1 well logs, the porosity derived from sonic velocity, and the sonic velocity from the RSU #1 well

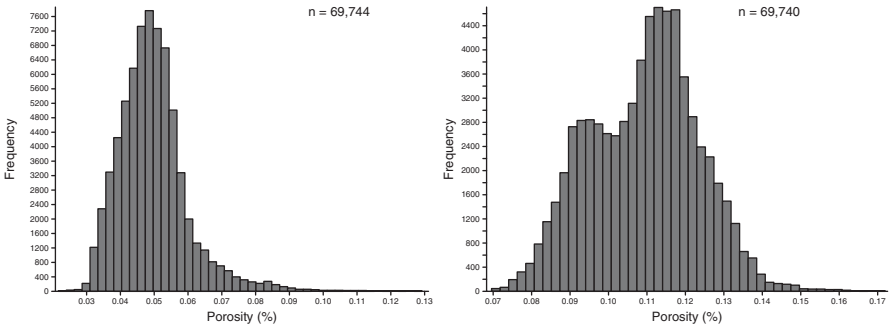

Fig. 10.17 Histograms of the porosity distributions of the Weber Sandstone (*left*) and Madison Limestone (*right*) within the Jim Bridger 3-D simulation domain

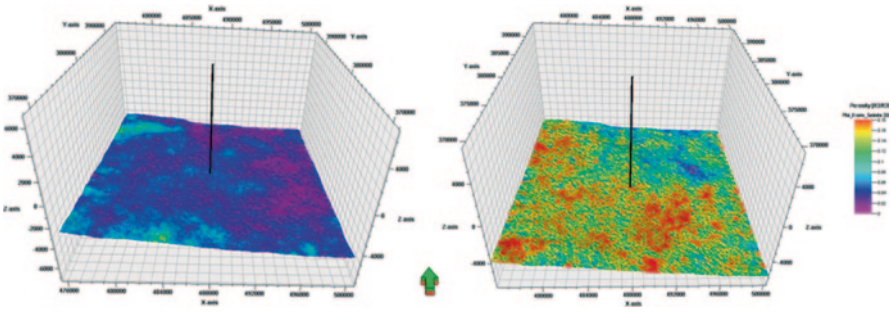

Fig. 10.18 The porosities derived from the seismic interval velocities for the Weber Sandstone (*left*) and the Madison Limestone (*right*) show significant heterogeneous characteristics in the geologic CO_2 storage simulation domain

simulation domain (Fig. 10.17b). The porosities of both the Weber Sandstone and Madison Limestone show significant heterogeneity. The Madison porosities derived from seismic interval velocities show a clear bi-modal distribution. This porosity volume is used in generating a 3-D permeability volume for the Jim Bridger geologic CO_2 storage simulation domain.

10.5.5 Permeability and Porosity

The permeability parameters are mapped from porosity through empirical correlations between porosity and permeability. The qualitative permeabilities determined in Chapter 9 were used to check porosity-permeabilities discussed below. Basically using the porosity/permeability cross plots discussed herein it was possible to quantify the high and low qualitative values determined in Chap. 9.

Three sets of porosity/permeability data for the Weber/Tensleep Sandstone collected from the region were utilized in this study (Fox et al. 1975; Bowker and

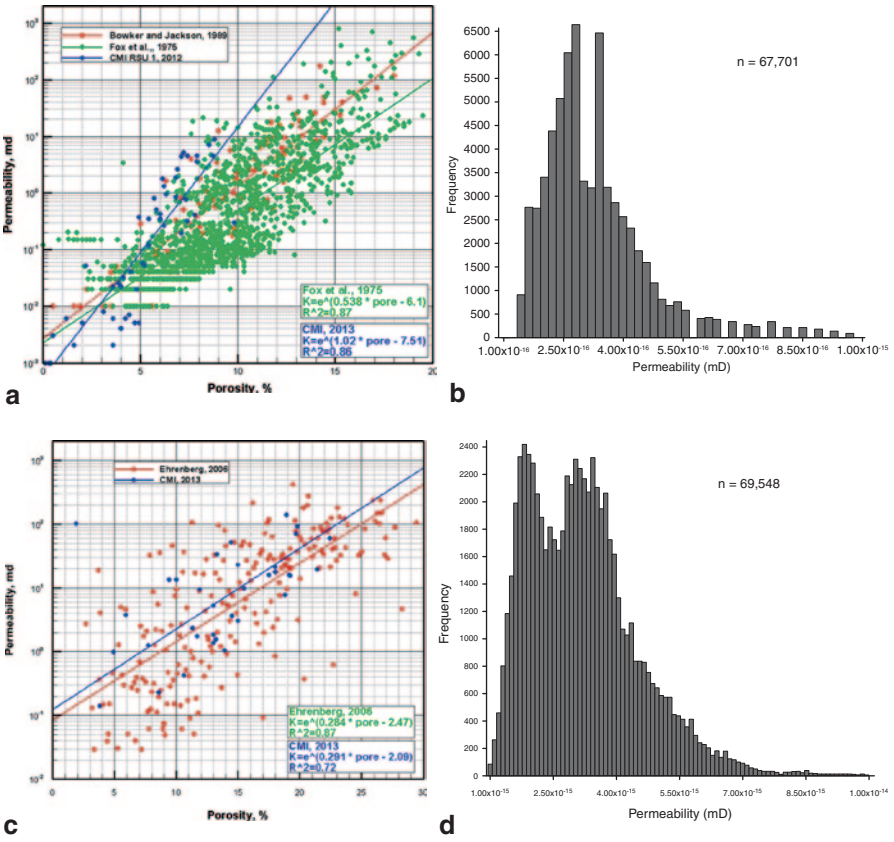

Fig. 10.19 (**a**) Plot of permeability vs. porosity in the Weber Sandstone, RSU and vicinity. All porosity and permeability data are laboratory measurements on core samples. (**b**) Permeability distribution of the Weber Sandstone in the Jim Bridger modeling domain. (**c**) Plot of permeability vs. porosity in the Madison Limestone, RSU and vicinity. (**d**) Permeability distribution of the Madison Limestone in the Jim Bridger modeling domain. The Madison permeability distribution is bimodal

Jackson 1989, and CMI 2013). The cross plot of porosity and permeability data for the Weber/Tensleep Sandstone samples is shown on Fig. 10.19a. The permeabilities measured in the RSU #1 core sample range from 0 to 10 mD. With a mean porosity of 5%, the permeabilities derived from the three sets of porosity data are fairly close, but in samples with the highest porosity the permeabilities can vary by an order of magnitude among the different data sets. For example, with the same porosity of 10%, the derived permeability is 0.6 mD from the Fox et al. (1975) dataset and 1.05 mD from a CMI research dataset. The Weber Sandstone on the RSU has higher permeabilities than those in the Weber/Tensleep Sandstone in the Wind River Basin and other areas of the Greater Green River Basin. The exponential function relating permeability k to porosity ϕ in the Weber Sandstone, derived by applying least-squares curve fitting to the CMI (2013) core-measured porosity/permeability dataset, is:

$$k = e^{1.02\Phi - 7.51}. \tag{10.2}$$

The other two empirical correlations for the Weber/Tensleep Sandstone of Fox et al. (1975) and Bowker and Jackson (1989) are shown on Fig. 10.19a for comparison. The CMI regression has a correlation coefficient $R^2 = 0.86$. The permeability volume of the Jim Bridger modeling domain was derived from the Jim Bridger porosity volume through Eq. 10.2. Figure 10.19b shows the distribution of the derived permeabities from 0 to 1 mD, which accounts for the permeabilities of 98 % of the simulation cells (67,615 of 69,147 cells) in the Weber Sandstone in the Jim Bridger modeling domain. The permeabilities in the Jim Bridger modeling domain range from 0.01 to 20 mD with a mean of 0.3 mD.

For the Madison Limestone, two sets of porosity/permeability datasets, from measurements on core samples from the RSU #1 well and the region, were available to this study (Ehrenberg 2006 and CMI 2013). The cross plot of porosity and permeability for the Madison Limestone samples is shown on Fig. 10.19c. The two datasets show similar trends for the relationship between the porosity and permeability. The permeabilities in the RSU #1 core samples range from 0.001 to 200 mD. An exponential function relating permeability k to porosity ϕ in the Madison was derived by applying least-squares curve fitting to the CMI (2013) core-measured porosity/permeability dataset:

$$k = e^{0.291\Phi - 2.09} \tag{10.3}$$

The Ehrenberg et al. (2006) empirical correlation for the Madison Limestone is shown on Fig. 10.19c for comparison. The CMI regression has a correlation coefficient of $R^2 = 0.72$. The permeability volume of the Jim Bridger modeling domain was derived from the Jim Bridger porosity volume by applying Eq. 10.3. Figure 10.19d shows distribution of the derived permeabilities in the Madison Limestone in the Jim Bridger modeling domain. These permeabilities range from 0.01 to 20 mD with a mean of 3 mD. The peameability of the Madison Limestone in the RSU has a bimodal distribution. The higher porosities and permeabilities are the result of the karst leaching, diagenesis, and microfracture development.

The primary containment formations for geologic CO_2 storage on the RSU are the Amsden Formation, Dinwoody Formation, and Red Peak Member of the Chugwater Formation. However the Cretaceous shale in the upper half of the stratigraphic section is more than 1,500 m thick and provides a multitude of secondary sealing sequences. The lithology of these Cretaceous containment formations is shale, mudstone, and carbonaceous shale. The permeability of the shale and clay-rich sandstone is a complex function of porosity, clay content, effective stress, and diagenesis (Yang and Aplin 2010). Because of the difficulty in making laboratory measurements on these lithologies, high-quality data on porosity and permeability in shale and mudstone is relatively rare (Neuzil 1994). In clay-rich lithologies, a simple linear regression relationship cannot capture a realistic relationship between porosity and permeability. In light of this complexity, this study used the empirical

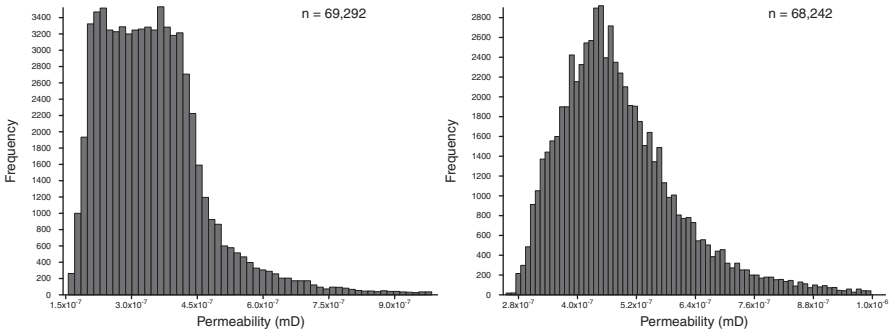

Fig. 10.20 Histograms showing the permeability distributions in the Dinwoody (*left*) and Chugwater (*right*) containment formations in the RSU geologic CO_2 storage simulation domain

correlation of Yang and Aplin (2010) to compute the permeability k of the sealing rocks with an assumed clay content C of 25 %:

$$\begin{aligned} \ln\ k = &-69.59 - 26.79C + 44.07C^{0.5} \\ &+\left(-53.61 - 80.03C + 132.78C^{0.5}\right)e \\ &+\left(86.61 + 91.91C - 163.61C^{0.5}\right)e^{0.5}, \end{aligned} \tag{10.4}$$

where k is the vertical permeability [m^2] ($m^2 \approx 10^{15}$ mD), C is the clay content [decimal fraction, here 0.25], $e = \phi/(1-\phi)$ is the void ratio [decimal fraction], and ϕ is the porosity [decimal fraction].

Figure 10.20 shows the permeability of the Dinwoody Formation and Chugwater Formation derived from the Jim Bridge 3-D porosity volume that was used in the RSU CO_2 storage simulations.

Modeled permeabilities are assumed to be isotropic for all facies and all rocks except the sealing rock, the Dinwoody and Chugwater formations, to which an anisotropic ratio of 10 was assigned (horizontal permeability is one order of magnitude greater than vertical permeability). The density of all rocks was fixed at 2,650 kg/m^3. The Joule-Thomson effect (Han et al. 2010) is included through conservation of enthalpy (Stauffer et al. 2003); however, the dry-out effect (Pruess and Muller 2009), geomechanical effects due to fluid pressure buildup, and geochemical reactions are not considered in the CO_2 injection simulations.

On the basis of the vertical extent of the borehole data acquired, the vertical heterogeneities are more fully captured than the horizontal ones. Yet, by combining geologic characterization and detailed 3-D seismic attribute analysis, the spatial (vertical and horizontal) heterogeneities in the simulations described herein are, we believe, as realisitic as is technically possible with the available dataset. The next step is to incorporate the spatial heterogeneities of porosity and permeability into the Jim Bridger 3-D seismic domain to simulate supercritical CO_2/brine multiphase fluid flow during CO_2 injection for 50 years with observation for 50 years post-injection, using the FEHM simulator.

Table 10.1 Parameters used for CO_2 injection simulations in the Weber Sandstone and Madison Limestone

Parameter	Symbol	Unit	Value	
			Weber	Madison
Saline aquifer effective permeability	k	m^2	Hetero	Hetero
Saline aquifer effective porosity	ϕ	%	Hetero	Hetero
Saline aquifer thickness	b	m	200	130
Saline aquifer salinity	s	%	11	8
Saline aquifer thermal conductivity	λ_m	W/Km	3.3	3.3
Saline aquifer initial fluid pressure	P_{inf}	MPa	31–40	34–43
Maximum temperature difference	T	°C	22	22
Brine viscosity	μ_w	Pa s	1.33×10^{-4}	1.33×10^{-4}
Brine density	ρ_w	kg/m^3	1,100	1,100
CO_2 fluid viscosity	μ_{CO_2}	Pa s	5.8×10^{-5}	$5.8x10^{-5}$
CO_2 fluid density	ρ_{CO_2}	kg/m^3	700	700
Brine compressibility	c_w	Pa^{-1}	3.5×10^{-10}	3.5×10^{-10}
CO_2 fluid compressibility	c_{CO_2}	Pa^{-1}	1.0×10^{-9}	1.0×10^{-9}
Pore compressibility	cp	Pa^{-1}	4.5×10^{-10}	4.5×10^{-10}
Injection time	t	year	50	50
Specific storage	S_s	–	5×10^{-6}	5×10^{-6}
Injection rate	Q	kg/s	constant	constant
Gravitational acceleration	g	m/s^2	9.8	9.8
Residual water saturation	S_{wr}	%	10	10
Maximum water saturation	S_{ws}	%	90	90
Residual CO_2 saturation	S_{CO_2r}	%	10	10
Maximum CO_2 saturation	S_{CO_2s}	%	90	90
Brine thermal expansion	λf	K − 1	0.001	0.001
Brine specific heat capacity	C_{pf}	J/kg K	4.2×10^3	4.2×10^3

10.5.6 Numerical Simulations of CO_2 Injection with Heterogenetic Reservoir and Containment Strata

10.5.6.1 Numerical Model Setup

The simulation domain is 8 km × 8 km × 3.6 km in the X, Y, and Z directions (width, length, and depth) and is discretized into 291,954 tetrahedral nodes with horizontal spacing of 150 m generally and 37.5 m near the injection well. The variable vertical resolution is reduced to 10 m in order to capture relatively small vertical correlation lengths in the Chugwater and Dinwoody, Phosphoria, Weber, Amsden, Madison, and Darby formations. The modeled formations dip is 5º northeast and the strike is 130º. Injection of CO_2 into the Weber Sandstone and Madison Limestone is assumed to be at a constant temperature (45 °C) and a constant injection pressure of 18.5 MPa (2,680 psi) at the well head. The injection pressure at the penetrated reservoirs is below 65 % lithostatic and is comparable to the maximum sustainable injection pressure estimated by Rutqvist et al. (2007), who analyzed coupled fluid flow and geomechanical fault-slip under conditions of hypothetical compression and extension stress. Important parameters of the CMI simulations are listed in Table 10.1.

The bottom of the simulation domain is a no-flow boundary. The top and up-dip (western and southern) boundaries of the simulation domain are open to flow in and out. The down-dip (northern and eastern) boundaries are closed. Constant temperatures are held at the top (55 °C) and bottom (147 °C) of the domain, which matches a geothermal gradient of 25.6 °C/km. The fixed side boundaries are used to allow an estimate of the amount of water that must be produced to ensure that the injection site does not impact surrounding parcels of land (i.e., land outside the 5 × 5-mi storage domain). Hydrostatic pressure and temperature fields are used as initial conditions for all simulations. The initial CO_2 fraction in injection well nodes is set at zero. These simulations incorporate a CO_2 density model (Duan et al. 2008) and a solubility model of CO_2 in brine (Duan et al. 2006) into their CO_2 transport modeling. Combined with thermodynamic updating, the density, viscosity, and solubility of CO_2 in the brine are simulated as temperature and pressure change.

10.5.6.2 CO_2 Injection into the Weber Sandstone (Heterogeneous Reservoir Model)

The results presented in this section are based on simulations that span 50 years of injection into one well completed in the Weber Sandstone using a realistic model of the Weber's heterogeneous reservoir properties. Fifty years of injection was chosen to simulate CO_2 storage because it corresponds to the typical lifetime of a coal-fired power plant in North America (Stauffer et al. 2009b). Porosity and permeability have a significant affect on injection feasibility. Injection rates of 1 Mt/yr, 0.75 Mt/yr, 0.5 Mt/yr, and 0.3 Mt/yr were simulated using the same heterogeneous reservoir model described above in Sect. 10.5, but only the rate of 0.3 Mt/yr of injection was feasible without inducing CO_2 migration across set lateral boundaries. The other, higher injection rates caused the simulations to terminate before the end of the 50-year period because of serious convergence errors or unacceptably high formation pressure. At 0.3 Mt/yr, 15 Mt CO_2 could be stored within the Weber Sandstone with a single injection well over a 50-year period. In order to keep the reservoir pressure below the hydro-fracture pressure, 19 Mt of formation water would have to be removed over the 50 year period (Fig. 10.21a). In the heterogeneous model the pressure changes are not uniformly distributed as in the homogeneity model, but instead occur mainly around the injection well, in the down-dip directions where the boundaries are closed. No unacceptable pressure elevations occur in the up-dip directions, where the boundaries are open to fluid migration (Fig. 10.21b).

Figure 10.21c is an oblique view and Fig. 10.21d a cross section of the injected CO_2 plume in the modeled Weber Sandstone after 50 years of injection at a rate of 0.3 Mt/yr. After 50 years of injection, the CO_2 plume remains within the Weber Sandstone reservoir and is irregularly shaped, covering an area of 10 km^2 (Fig. 10.21c). Unlike the CO_2 plume distributions in the homogeneous model, the CO_2 plume distributions in the heterogeneous model show a patchy pattern.

The storage capacity of the Weber Standstone for the entire RSU is estimated by assuming that the 3-D simulation domain is a representative element. Therefore,

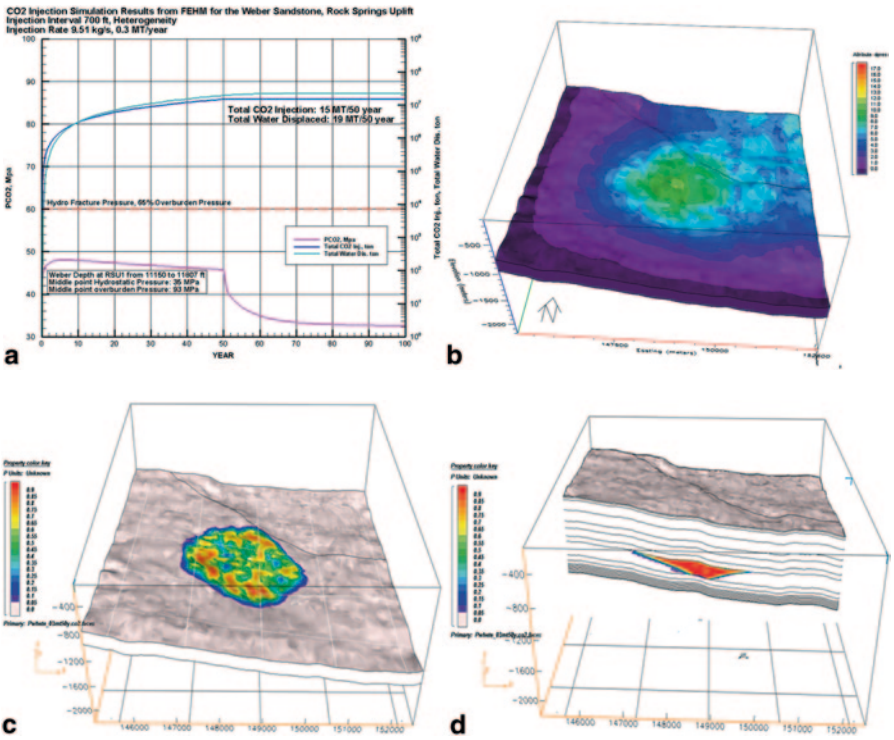

Fig. 10.21 (**a**) FEHM CO_2 injection simulation results for the Weber Sandstone, RSU. The simulation was set up for hetegogeneous reservoir conditions. The injection rate of 9.51 kg/s was constant for 50 years; then injection ceased, and the simulation ran for another 50 years without CO_2 injection. (**b**) The pressure regime of the Weber storage reservoir at the end of CO_2 injection. Depicted are the differences between the simulated reservoir hydrostatic pressure and the simulated reservoir pressure at the end of 50 years of CO_2 injection. (**c**) Oblique view and (**d**) cross section of the CO_2 plume in the Weber Sandstone representing the 15 Mt of CO_2 injected into the reservoir by the end of 50 years of CO_2 injection

once the volume V_{plume} of the CO_2 plume in the simulation domain and the volume V_{RSU} of the Weber Sandstone in the whole RSU are known, a simple approximation of the storage capacity C can be calculated by Eq. 10.5:

$$C = \left(\frac{V_{RSU}}{V_{plume}} \right) \times M_{CO_2} \tag{10.5}$$

where M_{CO_2} is the total mass of CO_2 injected into the saline aquifer in the simulation domain over 50 years. The CO_2 plume with saturations from 0.05 to 0.9% fills a volume of 0.65 km^3 with 15 Mt of CO_2. The total volume of the Weber Sandstone above depth of 5,000 m within the RSU is 412 km^3. Therefore, if all the Weber Sandstone on the RSU were used for the storage, the storage capacity of the Weber on the RSU could be as great as 9.5 Gt of CO_2.

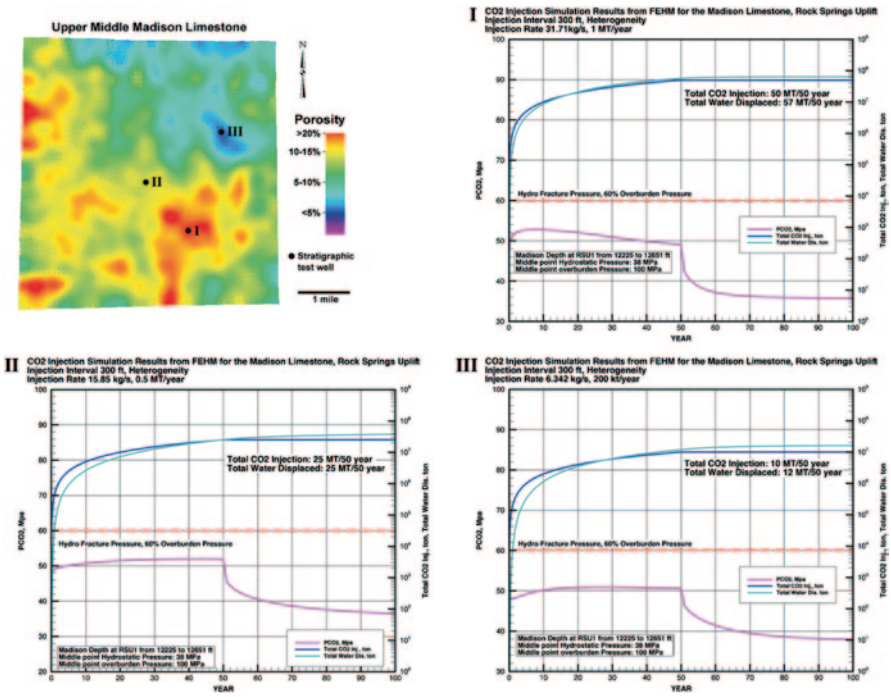

Fig. 10.22 FEHM CO_2 injection simulation results for the Madison Limestone, RSU. The simulations were set up for heterogeneous reservoir conditions. The injection rates of 31.71, 15.85 and 6.34 kg/s were constant for 50 years for wells in the high (**I**), medium (**II**), and low (**III**) reservoir-quality areas, respectively. The injections continued for 50 years, then ceased, and the simulations ran for another 50 years without CO_2 injection. The reservoir pressure elevated quickly when injection started, but was below the hydro-fracture pressure throughout injection. After injection ceased, the reservoir pressure fell back to near the original pressure within 10 years

10.5.6.3 CO_2 Injection into the Madison Limestone

The main reservoir-property heterogeneities in the Madison Limestone on the RSU are in porosity and permeability. The porosities within the modeling domain range from less than 1% to more than 20%, and permeabilities range from 0.001 mD to more than 100 mD. The numerical simulations used an injection interval of 76 m (250 ft) in the middle Madison Limestone. Three wells located in the high, medium, and low reservoir-quality areas in the storage domain were chosen to evaluate the injectivity and storage capacity of the Madison Limestone on the RSU (Fig. 10.22a**).**

After simulated injection started, the fluid pressure increased immediately at the injection well to 50% of overburden pressure. In the higher reservoir-quality case (well I), the fluid pressure field reached a quasi-steady state about four years after injection began, then decreased gradually (Fig. 10.22b). However, in the medium and low reservoir-quality cases (wells II and III) the pressure evolved gradually over the 50-year injection period (Fig. 10.22c, d). The fluid pressure increased mainly

in the injection zone, with an increase in pressure of between 1 MPa (145 psi) and 17 MPa (2,470 psi) in the middle Madison.

Concurrently with the pressure increase at the start of injection, the CO_2 plumes began to grow and migrate. At the end of 50 years of injection the supercritical CO_2 plumes had expanded away from the injection wells, with preferential flow toward the up-dip open boundaries (Fig. 10.23b, e, h). The CO_2 plumes did not grow uniformly in either the horizontal or the vertical direction, because of heterogeneity, pressure interference, and the dip of the formation. In all three simulations the CO_2 plume migrated away from the injection well in the up-dip direction and developed a long, narrow front at the top of the Madison Limestone (Fig. 10.23d, g, j). In all three locations, formation water had to be displaced to create accommodation space for the injected CO_2 and to keep the reservoir pressure below the hydro-fracture pressure. Also for the three injection scenarios, the reservoir pressure increased rapidly at the start of injection, but quickly decreased to near the reservoir hydrostatic pressure within 10 years after the injection ceased (Fig. 10.22b, c, d).

The injectivity and storage capacities are significantly different among high, medium, and low reservoir-quality areas. In a high reservoir-quality reservoir 50 Mt CO_2 could be injected and safely stored in the Madison Limestone over a 50 year period, with an injection rate of 31.71 kg/s and 57 Mt of formation fluid displaced (Fig. 10.22b, well I). In a medium reservoir-quality reservoir, to keep the reservoir pressure below the fracture pressure, only 25 Mt CO_2 could be injected and safely stored in the Madison over a 50-year period, with an injection rate of 15.85 kg/s and 25 Mt of formation fluid displaced (Fig. 10.22c, well II). In a low reservoir-quality reservoir, just 10 Mt CO_2 could be injected and safely stored in the Madison Limestone over a 50 year period, with an injection rate of 6.34 kg/s and 12 Mt formation water displaced (Fig. 10.22d, well III). In all cases, the amount of displaced fluid was of the same order of magnitude as the amount of CO_2 injected into the reservoirs.

The plumes of injected CO_2 differ among the high, medium, and low reservoir-quality areas where the injection wells were located (Fig. 10.23a). The results differ from those in the homogeneous reservoir case a common in the heterogeneous case a CO_2 plume at the top of the Madison Limestone exhibits an irregular shape and spreads to the left (up-dip direction), through relatively higher porosity and permeability zones toward the open boundary (Fig. 10.23b, e, h). As expected, all CO_2 plumes show the expansion at the plume top because of buoyancy-driven spreading along the base of the lower-permeability unit above the Madison (the Amsden Formation) (Fig. 10.23d, g, j). None of the simulated supercritical CO_2 plumes have not crossed the domain boundary in 50 years of injection (64 km^2).

The differences in the amount of CO_2 stored in the high, medium, and low reservoir-quality zones after 50 years of injection reflects significant differences in the porosity and permeability distribution within the middle Madison Limestone (Fig. 10.23a). Because no CO_2 has leaked into the overlying Amsden Formation in these simulations, the storage capacity of the Madison is defined on the basis of the amount of CO_2 injected over 50 years *separately for each simulation*. Using Eq. 10.5, the storage capacity of the Madison Limestone for the entire RSU is esti-

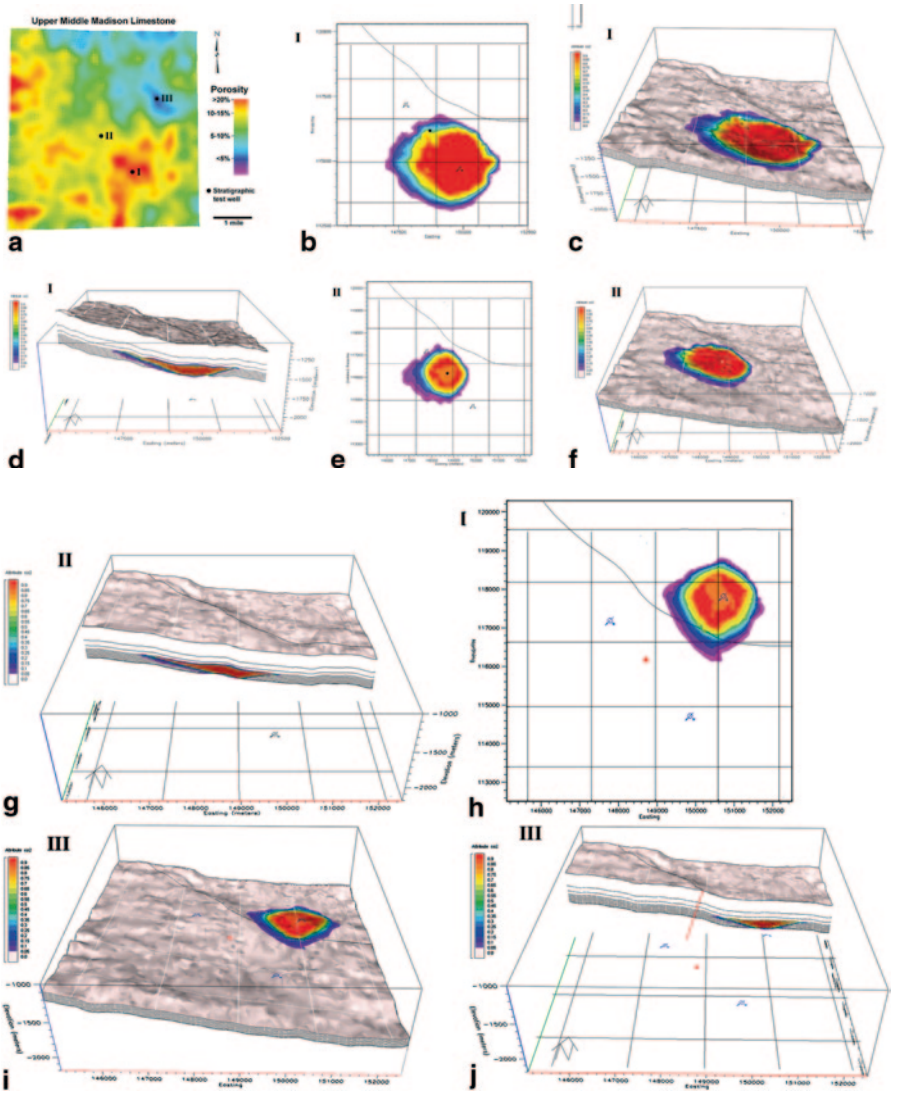

Fig. 10.23 (**a**) Heterogeneous porosity distrubion in the Madison Limestone within the RSU modeling domain and locations of the high (*I*), medium (*II*) and low (*III*) reservoir-quality areas chosen for simulation. These simulations used an injection interval of 400 ft (122 m). The grids represent section boundaries. (**b**) Map, (**c**) oblique, and (**d**) sectional views of the CO_2 plume in the Madison Limestone after 50 years of CO_2 injection into a high reservoir-quality area at a rate of 1.0 Mtyr. (**e**) Map, (**f**) oblique, and (**g**) sectional views of the CO_2 plume in the Madison after 50 years of CO_2 injection into the medium reservoir-quality area at a rate of 0.5 Mtyr. (**h**) Map, (i) oblique, and (j) sectional views of the CO_2 plume in the Madison after 50 years of CO_2 injection into the low reservoir-quality area at a rate of 0.2 Mt/yr

mated by assuming that the 3-D simulation domain (5 mi × 5 mi, 8 km × 8 km) is a representative element of the RSU (35 mi × 50 mi, 56 km × 80 km). The CO_2 plume volumes are 1.1 km^3 in the high reservoir-quality case (Fig. 10.23c, d), 0.642 km^3 in the medium reservoir quality-case (Fig. 10.23f, g), and 0.337 km^3 in the low reservoir-quality case (Fig. 10.23i, j). A volume 179 km^3 for the Madison Limestone above a depth of 5,000 m on the whole RSU is derived from the RSU geologic structural model constructed using EarthVision® geospacial modeling software (Fig. 10.2). For the high reservoir-quality case, the Madison Limestone on the RSU can store 8 Gt of CO_2; for the medium reservoir-quality case, 7 Gt of CO_2; and for the low reservoir-quality case, 5 Gt of CO_2. Thus under this set of simuations that account for porosity and permeability heterogeneity, the storage capacity of the Madison Limestone on the RSU is between 5 Gt and 8 Gt, the weighted average value depending on the volumetric proportions of the high, medium, and low reservoir-quality zones.

10.6 Comparison of Methods to Assess CO_2 Storage Capacity

The work presented in this chapter affords the opportunity to discuss the strengths and weaknesses of each of the three analytical methods: the static volumetric model, dynamic homogenous reservoir model, and dynamic heterogeneous reservoir model. The volumetric model is based on regional data for the average values of key parameters such as thickness, porosity, and permeability. The dynamic reservoir model is based on the measured thickness of reservoir intervals (site-specific well logs), average values of porosity and permeability derived from the laboratory measurements, and injectivity and other fluid-flow measurements from the well bore of the site-specific stratigraphic test well. The dynamic heterogeneous reservoir model is based on the well-bore measured thickness of each lithofacies in each of the reservoir intervals; detailed diagenetic, fluid chemistry, and geochemical studies of specific depositional facies in each of the reservoir intervals; injectivities measured in the well-bore; and, most importantly, laboratory-measured porosities and permeabilities correlated with seismic attributes in order to construct a 3-D model of reservoir petrophysical heterogeneity at and away from the well bore.

In this progression of evaluation methodology there is an inherent decrease in geologic uncertainty. Figure 10.24 compares the three methods for estimating CO_2 storage capacity as applied to the Weber Sandstone and Madison Limestone in the 5-mi × 5-mi (8-km × 8-km) storage domain on the RSU. The volumetric method suggests that 793 Mt of CO_2 can be stored in the Weber and Madison reservoir interval in the storage domain, whereas the dynamic homogeneous reservoir model suggests that this same reservoir interval can store 655 Mt of CO_2. In marked contrast, the numerical simulations for the same storage domain and reservoir interval using the dynamic heterogeneous reservoir model suggests that the Weber Sandstone and Madison Limestone can store 303 Mt of CO_2. If the dynamic model that

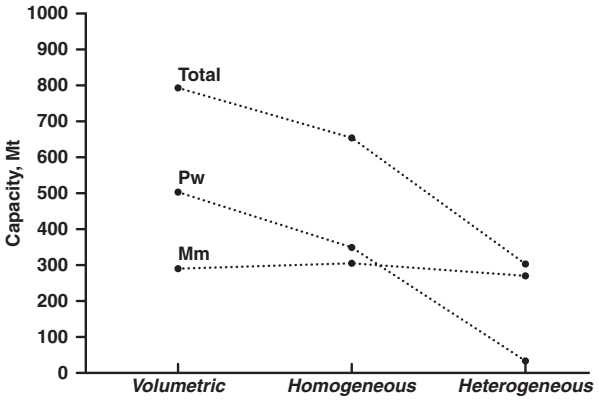

Fig. 10.24 Comparisons of CO_2 storage capacity in the Weber Sandstone (Pw) and Madison Limestone (Mm), and their total capacity, as estimated using a static volumetric model, a dynamic reservoir model , and a dynamic heterogeneous reservoir model

considers the 3-D reservoir heterogeneity is the most realistic configuration of the reservoir interval, then it follows that the volumetric approach overestimates the reservoir storage capacity by a factor of 2.5. Comparing the numerical simulations of the two dynamic reservoir models, the homogeneous model overestimates CO_2 storage capacity by a factor of 2.2. Of course, the volumetric approach requires less time and effort, and dynamic simulations with the heterogeneous reservoir model require the most effort and the most data.

For reliable, low-risk evaluations of potential CO_2 storage sites, it is imperative to use 3-D reservoir models that include the heterogeneity of petrophysical, diagenetic, and geochemical distributions away from the boreholes within the storage domain. To achieve estimates of CO_2 storage capacity for targeted reservoir intervals, data from at least one stratigraphic test well and a 3-D seismic survey over the storage domain are probably essential. Without this site-specific data, risk and performance assessments of CO_2 storage scenarios remain plagued by unacceptable uncertainty.

10.7 Conclusions

- Reducing geologic uncertainty in evaluations of geologic CO_2 storage site scenarios requires a robust database that allows an accurate reconstruction of the targeted storage rock/fluid volume, especially with respect to spatial petrophysical heterogeneities. Results that rely on a generalized regional database to populate a homogenous rock/fluid volume based on average reservoir properties yields general insights into injection/storage characteristics but lacks specificity, resulting in performance assessments plagued by substantial uncertainty. To move from idealistic, highly generalized assessments to realistic, low-risk assessments of the Rock Springs Uplift, it was necessary to acquire high-resolution data specific to the storage site of interest.
- The integration of the 3-D seismic and well log data—along with visual observations from the core—has substantially reduced the uncertainty attached to per-

formance assessments and risk analysis for the RSU storage site characterization project (WY-CUSP). As the new data from laboratory analyses, experimental determinations, and test evaluations become available and are integrated into the RSU property models, uncertainty, particularly with respect to reservoir property heterogeneity was further reduced. This study establishes an exemplary strategy for dealing with CO_2 storage projects in relatively deep saline aquifers in the Rocky Mountain region and elswhere.

- Reservoir heterogeneity has a significant affect on the geologic CO_2 injection rates and storage capacity of the targeted saline aquifers. Applying the diagnostic protocol for the CO_2 sequestration suggested by Department of Energy for the FutureGen project, the CO_2 storage capacity of the Weber Sandstone in the RSU was estimated to be 18 Gt (Surdam and Jiao 1997). Appling the volumetric approach proposed by the U. S. Geologic Survey, the CO_2 storage capacity of the Weber Sandstone was estimated to be 9 GT with the probability density ranging from 2.4 to 20 Gt. Using the FEHM multi- flow numerical simulator, the CO_2 storage capacity of the Weber Sandstone was estimated to be 17 Gt based on the homogeneous reservoir property model (porosity 10%, permeability 1 mD), and 9.5 Gt based on the heterogeneous reservoir property model. The 2.1-GW Jim Bridger Power Plant located a mile from the simulation injection well emits 15 Mt of CO_2 annually. Therefore, the Weber Sandstone reservoir in the RSU is capable of storing the CO_2 emitted from Jim Bridger Power Plant for 600 years.
- For the Madison Limestone reservoir in the RSU, the geologic CO_2 storage capacity was estimated to be 8 Gt using the protocol of the FutureGen project suggested by the Department Energy. Using the USGS volumetric approach, the probability density of the CO_2 storage capacity of the Madison Limestone ranges from 1.6 to 14 Gt, with a mean of 6.5 Gt. Using the FEHM multi flow numerical simulator, the CO_2 storage capacity of the Madison Limestone was estimated to be 7 Gt for the homogeneous reservoir property model (porosity 10%, permeability 1 mD). Based on the heterogeneous reservoir property model, the CO_2 storage capacity of the middle Madison Limestone in the RSU area was estimated to be 8 Gt for the high reservoir-quality domain, 7 Gt for the medium reservoir-quality domain, and 5 Gt for the low reservoir-quality domain. Using results from the CO_2 injection simulation for the medium reservoir-quality case, the Madison Limestone could store the CO_2 emissions from the Jim Bridger Power Plant for 460 years.
- Well injection rate is highly dependent on the local permeability distribution in the storage formation. The areas and interval with the higher quality reservoir domains are critical for a successful commercial-scale geologic CO_2 storage project. The higher-quality reservoir domains substantially reduce the project cost and significantly increase the CO_2 injectivity and storage capacity. For the middle Madison Limestone and selected intervals in the Weber Sandstone with higher-quality reservoir domains, the injection rate can be as high as 1 Mt per year, while in the lower-quality reservoir domains, the injection rate can be as low as 0.2 Mt per year.

- Formation brine is displaced by CO_2 in the injection simulations in order to keep formation pressure below the hydro-fracture pressure, reduce associated leakage, decrease seismic risk, and create the accommodation space to enhance storage capacity for CO_2. It is proposed that brine displacement be allowed and controlled by production at the land surface through production wells on the perimeter of the storage site. The average ratio of the amount (tonnage) of displaced brine to injected CO_2 is 1.14. This ratio indicates that for an industrial-scale CO_2 injection project with minimal impact on neighboring pore space a little more brine must be displaced than CO_2 injected.
- CO_2 leakage from the storage formations into the overlying rocks is related to the connectivity of high-permeability layers. Leakage from the Madison limestone into the overlaying Amsden Formation is minimal owing to the lower permeability characteristics of the Amsden. However, migration from the Weber into the Phosphoria is significant. This result implies that the Phosphoria should be considered a secondary storage unit, not a cap-rock, on the RSU. In strong contrast, no CO_2 injected into either the Weber or Madison migrated into the primary cap rocks of the overlying Dinwoody Formation. The sealing capacity of the Dinwoody Formation can be as great as a 2,000-ft gas column.

References

Bowker KA, Jackson WD (1989) The Weber Sandstone at Rangely Field, Colorado. In: Coalson EB et al. (eds) Petrogenesis and petrophysics of selected sandstone reservoirs of the Rocky Mountain region. Rocky Mountain Association of Geologists, p 65–80

Burruss RC, Brennan ST, Freeman PA, Merrill MD, Ruppert LF, Becker MF, Herkelrath WN, Kharaka YK, Neuzil CE, Swanson SM, Cook TA, Klett TR, Nelson PH, and Schenk CJ (2009) Development of a probabilistic assessment methodology for evaluation of carbon dioxide storage. U.S. Geologic Survey Open File Report 2009–1035

Clarey K, Thompson M (2010) Chapter 2, study area. In: Copeland D, Ewald M (eds) Available groundwater determination technical memorandum [Greater Green River Basin]. Report prepared for the Wyoming Water Development Commission by the Wyoming State Geologic Survey et al. Wyoming State Geologic Survey, Laramie, p 2-1–2–25

Duan Z, Sun R, Zhu C, Zhou IM (2006) An improved model for the calculation of CO_2 solubility in aqueous solution containing Na^+, K^+, Ca^{2+}, Mg^{2+}, Cl^-, and SO_4^{2-}. Mar Chem 98:131–139

Duan Z, Hu J, Li D, Mao S (2008) Densities of the CO_2-H_2O and CO_2-H_2O-NaCl systems up to 647 K and 100 MPa. Energy Fuels 22:1666–1674

Ehrenberg SN, Eberli GP, Keramati M, Moallemi SA (2006) Porosity-permeability relationships in interlayered limestone-dolostone reservoirs. AAPG Bull 90:91–114

Fox JE, Lambert PW, Mast RF, Nuss NW, Rein RD (1975) Porosity variation in the Tensleep and its equivalent, the Weber Sandstone, western Wyoming: a log and petrographic analysis. Rocky Mt Assoc Geol 12:185–215

Han WS, Stillman GA, Lu M, Lu C, McPherson BJ, Park E (2010) Evaluation of potential nonisothermal processes and heat transport during CO_2 sequestration. J Geophys Res 115:B07209. http://dx.doi.org/10.1029/2009JB006745

Hein JR, Perkins RB, McIntye BR (2004) Evolution of thought concerning the origin of the Phosphoria Formation, western US phosphorate field. In: Hein JR (ed) Life cycle of the Phosphoria Formation: from deposition to post-mining environment. Elsevier, p 19–42

Love JD, Christiansen AC, Ver Ploeg AJ (1993) Stratigraphic chart showing Phanerozoic nomenclature for the state of Wyoming. Wyo State Geol Surv Map Ser 41:(MS–41)

Miller TA, Vessilinov VV, Stauffer PH, Birdsell KH, and Gable CW (2007) Integreation of geologic frameworks in meshing and setup of computational hydrogeologic models, Pajarito Plateau, New Mexico. New Mexico Geologic Society Guide Book, 58th Field Conference, Geology of the Jemez Mountains Region III

Neuzil CE (1994) How permeable are clays and shales? Water Resour Res 30:145–150

Piper DZ, Link PK (2002) An upwelling model for the Phophoria sea: a Permian, ocean-margin sea in the northwest United States. AAPG Bull 86(7):1217–1235

Pruess K, Muller N (2009) Formation dry-out from CO_2 injection into saline aquifers: 1. Effects of solid precipitation and their mitigation. Water Resour Res 45:W03402. http://dx.doi.org/10.1029/2008WR007101

Stauffer PH, Stein JS, Travis BJ (2003) The correct form of the energy balance for fully coupled thermodynamics in water. Los Alamos National Laboratory Report, LA-UR-03-1555, p 9

Stauffer PH, Surdam RC, Jiao Z, Miller TA, Bentley RD (2009a) Combining geologic data and numerical modeling to improve estimates of the CO_2 sequestration potential of the Rock Springs Uplift, Wyoming. Energy Procedia 1:2717–2724

Stauffer PH, Viswanathan HS, Pawar RJ, Guthrie GD (2009b) A system model for geologic sequestration of carbon dioxide. Environ Sci Technol 43:565–570

Surdam RC, Jiao Z (2007) The Rock Springs uplift: an outstanding geologic CO_2 sequestration site in southwest Wyoming. Wyoming State Geologic Survey Challenges in Geologic Resource Development No. 2

Surdam RC, Jiao Z, Stauffer PH, Miller T (2009) An integrated strategy for carbon management combing geologic CO_2 sequestration, displaced fluid production, and water treatment. Wyoming State Geologic Survey Challenges in Geologic Resource Development No. 8

Yang Y, Aplin AC (2010) A permeability-porosity relationship for mudstone. Mar Petrol Geol 27:1692–1697

Zyvoloski GA, Dash ZV, Kelkar S (1988) FEHM: finite element heat and mass transfer code. Los Alamos National Laboratory Report LA-11224-MS. NNA.19900918.0013

Zyvoloski GA, Robinson BA, Dash ZV, Trease LL (1997) Summary of the models and methods for the FEHM application—a finite element heat-and mass-transfer code. Los Alamos National Laboratory Report LA-13307–MS